INVESTIGATION OF MECHANICAL AND METALLURGICAL PROPERTIES OF SHAPE MEMORY NITINOL BASED WIRES

Abubaker J. Amir IRHAYIM

2021
MASTER THESIS
MECHANICAL ENGINEERING

Thesis Advisor
Assoc. Prof. Dr. İsmail ESEN

INVESTIGATION OF MECHANICAL AND METALLURGICAL PROPERTIES OF SHAPE MEMORY NITINOL BASED WIRES

Abubaker J. Amir IRHAYIM

T.C.
Karabuk University
Institute of Graduate Programs
Department of Mechanical Engineering
Prepared as
Master Thesis

Thesis Advisor
Assoc. Prof. Dr. İsmail ESEN

KARABUK
March 2021

I certify that in my opinion the thesis submitted by Abubaker J. Amir IRHAYIM titled "INVESTIGATION OF MECHANICAL AND METALLURGICAL PROPERTIES OF SHAPE MEMORY NITINOL BASED WIRES" is fully adequate in scope and in quality as a thesis for the degree of Master of Science.

Assoc. Prof. Dr. İsmail ESEN .....
Thesis Advisor, Department of Mechanical Engineering

This thesis is accepted by the examining committee with a unanimous vote in the Department of Mechanical Engineering as a Master of Science thesis. March 26, 2021

Examining Committee Members (Institutions)	Signature
Chairman : Assoc. Prof. Dr. İsmail ESEN (KBU)	.....
Member : Assoc. Prof. Dr. Selami SAGIROGLU (KBU)	.....
Member : Assist. Prof. Dr. Mehmet Akif KOÇ (SUBU)	.....

The degree of Master of Science by the thesis submitted is approved by the Administrative Board of the Institute of Graduate Programs, Karabuk University.

Prof. Dr. Hasan SOLMAZ .....
Director of the Institute of Graduate Programs

"I declare that all the information within this thesis has been gathered and presented in accordance with academic regulations and ethical principles and I have according to the requirements of these regulations and principles cited all those which do not originate in this work as well."

Abubaker J.Amir IRHAYIM

ABSTRACT

M. Sc. Thesis

INVESTIGATION OF MECHANICAL AND METALLURGICAL PROPERTIES OF SHAPE MEMORY NITINOL BASED WIRES

Abubaker J. Amir IRHAYIM

Karabük University
Institute of Graduate Programs
The Department of Mechanical Engineering

Thesis Advisor:
Assist. Prof. Dr. İsmail ESEN
March 2021, 69 pages

Shape memory materials are "smart" materials and have the ability to absorb energy in the charge and discharge cycle. The most commonly used alloys today are based on those based on copper and nickel titanium (Ni-Ti), such as Cu-Al-Be or Cu-Al-Zn. Nitinol (nickel-titanium alloy) is a shape memory alloy that can be used for applications in many medical devices due to its good mechanical properties, good heat and corrosion resistance, and high energy dissipation capacity. Also, being recyclable makes it a good material for many engineering applications. The ability of nickel-titanium alloys to regain their initial state after stretching depends on the deformation and temperature of the material. If the material undergoes deformation at low temperatures, it can return to its original shape by increasing its temperature above a certain level called Af (end of the austenitic phase), and if it deforms at high temperatures, the material takes its shape instantly. In the second case, it is called superelastic material.

Generally, this shape is memorized after being shaped at a high temperature. This temperature is called memory temperature. If it is then deformed at the application temperature, usually room temperature or a certain low temperature, it returns to the previously memorized shape. Shape memory alloys are relatively new for medical applications, so there is little experience in using these materials. In this study, the mechanical behavior of a 1.5 mm diameter Nitinol wire was experimentally investigated.

Keywords **:** Nitinol wire, smart materials, characterization.
Science Code : 91421

ÖZET

Yüksek Lisans Tezi

ŞEKİL HAFIZALI NİTİNOL ESASLI TELLERİN MEKANİK VE METALURJİK ÖZELLİKLERİNİN İNCELENMESİ

Abubaker J. Amir IRHAYIM

Karabük Üniversitesi
Lisansüstü Eğitim Enstitüsü
Makina Mühendisliği Anabilim Dalı

Tez Danışmanı:
Doç. Dr. İsmail ESEN
Mart 2021, 69 sayfa

Şekil hafızalı malzemeler "akıllı" malzemeler olup, şarj ve deşarj döngüsünde enerjiyi emme özelliğine sahiptirler. Günümüzde en yaygın olarak kullanılan alaşımlar, Cu-Al-Be veya Cu-Al-Zn gibi bakır ve nikel titanyum (Ni-Ti) esaslı olanlara dayanmaktadır. Nitinol (nikel-titanyum alaşımı), iyi mekanik özelliklere sahip olması, iyi ısı ve korozyon direncine sahip olması ve yüksek nerji yayılma kapasitesine sahip olması nedeniyle birçok tıbbi cihazında kullanılabilen uygulamalar için kullanılabilen bir şekil hafızalı alaşımdır. Ayrıca geri dönüştürülebilir olması, onu pek çok mühendislik uygulaması için iyi bir malzeme yapar. Nikel-titanyum alaşımlarının gerilmeden sonra ilk durumlarını geri kazanma yeteneği, malzemenin deformasyonuna ve sıcaklığına bağlıdır. Malzeme düşük sıcaklıklarda deformasyona uğrarsa, Af denilen belirli bir seviyenin üzerine çıkarak (östenitik fazın sonu) sıcaklığını artırarak orijinal şekline dönebilir ve yüksek

sıcaklıklarda deformasyona uğrar ise malzeme anında şeklini alır. İkinci durumda, süper elastik malzeme olarak adlandırılır.

Genellikle yüksek bir sıcaklıkta şekillendirildikten sonra bu şekil hafızaya alınır bu sıcaklığa hafıza sıcaklığı denir. Daha sonra uygulama sıcaklığında genellikle oda sıcaklığı veya belirli düşük bir sıcaklıkta deforme edilirse, daha önceden hafızaya alınan şekle geri döner. Şekil hafızalı alaşımlar, tıbbi uygulamalar için nispeten yenidir, bu nedenle bu malzemeleri kullanma konusunda çok az deneyim vardır. Bu çalışmada, 1.5 mm çapında Nitonol bir telin mekanik davranışı deneysel olarak incelenmiştir.

Anahtar Kelimeler : Nitinol tel, akıllı malzemeler, karekterizasyon.
Bilim Kodu : 91421

ACKNOWLEDGMENT

I would like to thank my advisor, Assoc. Prof. Dr. İsmail ESEN, for his great interest as well as assistance in preparation of this thesis.

CONTENTS

Page

Page

Page

LIST OF FIGURES

Page

Page

Page

LIST OF TABLES

Page

PART 1

INTRODUCTION

1.1. SHAPE MEMORY ALLOYS HISTORY

Ah. Olander found the discovery of shape memory alloys in 1930 when was working on the Au-47.5at% Cd alloy and discover its pseudo elastic behavior. In 1938, Mooradian and Greninger discovered the formation phenomenon and disappearance in Cu-Zn alloy; martensitic phase by varying the temperature. Because, it was discovered in in Naval Ordnance Laboratory, So Nitinol they called it (Nickel-Titanium Naval Ordnance Laboratory) [1]. Only some of alloy are present in the market because most of them are expensive and not compatible unless in crystal form but Nitinol and CuZnAl are also present commercially. Because they are inexpensive and safer than other shape memory alloys. In 1932, A. Olander first discovered the phenomenon of form memory in gold-cadmium alloys. In 1940, he investigated pseudoelasticity and in Cu-Zn and indium thallium alloys the same effect was found. Khandros and Kurdumov discovered the source of this effect; the reversible martensitic phase transformations are dependent on temperature.

In the following years, the study on Nitinol and metallurgical testing established the thermomechanical properties of this alloy [2]. By characterizing the properties and the basic phenomenon of martensitic phase transformation the Nitinol alloy was considerably used in various high potential applications. Nitinol alloy was firstly used in Cryofit coupling ring and also used for Gumman F-14 Tomcat aircraft as a hydraulic pipelines by the Rayehem. Nitinol gets hug attention due to its unexpected properties and developing trend in aerospace, biomedical and robotic applications.

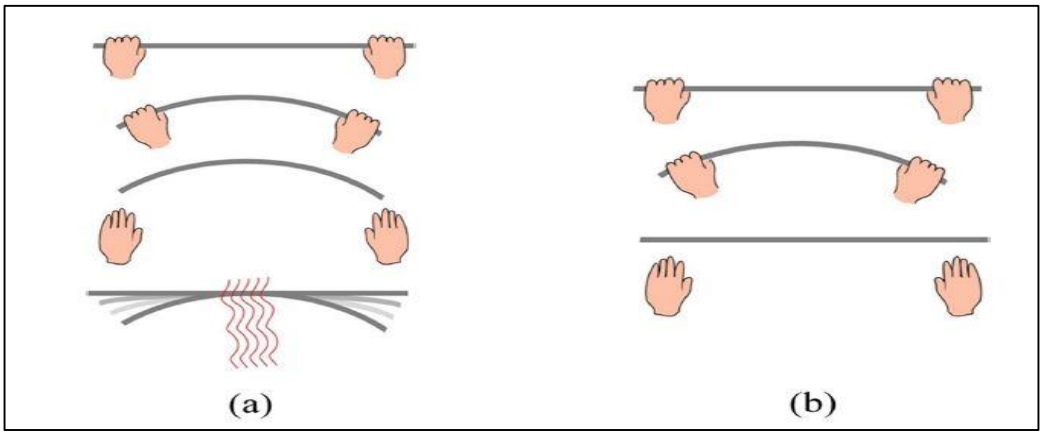

Figure 1.1. The above figure is (a) Shape memory and its effect, (b) Shape memory alloys and the amount of elasticity [2].

Step Transition in Shape Memory Alloy it is clear from the above the group of SMAs spans due to applications in vast area of metallic elements and their structures (crystal structure). (A) Plays the high temperature and low-temperature transition process martensite. Martensite is usually a lower degree of crystal-structural symmetry such as orthorhombic, tetragonal, monoclinical or hexagonal but has a high degree of crystal-structural symmetry which includes the cubic. Predictably the phase transformation occurred due to heating is Martensite to austenite (M-A) and phase transformation present due to cooling is called austenite to martensite (A-M) also known as forward transformation but the M-A transformation is called as reverse transformation [3].

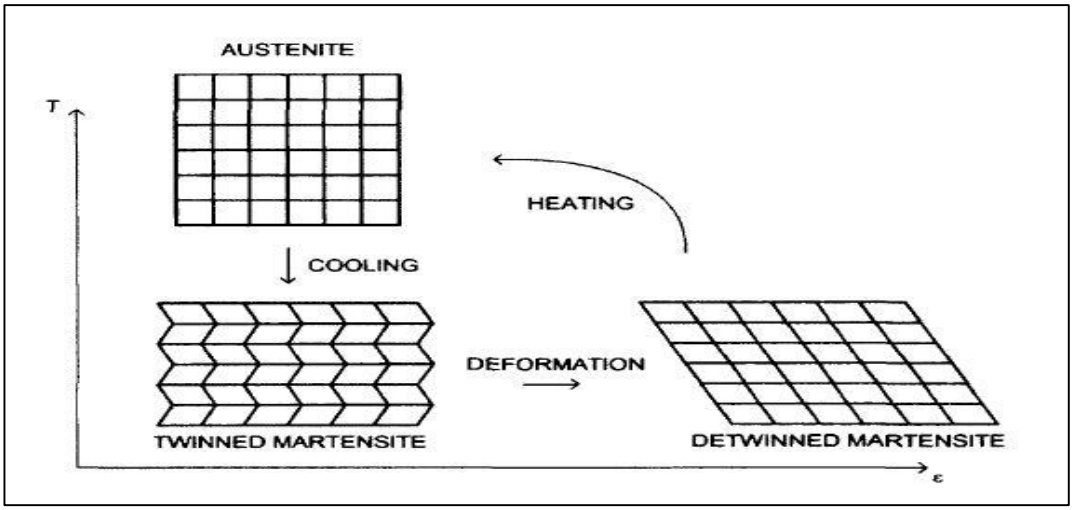

Figure 1.2. Super elasticity process [4].

The martensitic phase transformation is diffusion less phenomenon by which crystal structure of austenite concerted into the martensite crystal structure. The atomic movement and lattice distortions are responsible for this. Because of the diffusion of the unit cell, the conversion of a crystal form is formed. From this the martensitic phase transformation is change in crystalline transformation in structure and mechanical deformation in crystal [5]. By giving the mechanical limitations to transforming body, these shapes change behavior housed in the body to allow the phase transformation to proceed. In the martensitic phase transformation, there are two basic procedures: 1st with plastic deformation as shown in Figure 1.2 forming martensitic plates in various dimensions as shown in Figure 1.2. Clearly, the process is irreversible and so non-thermoelastic and latter it is reversible, and it becomes thermoelastic and it is called as the shape memory alloy has thermoelastic martensitic phase transformation. Different dimensions of martensite plates but same crystal structure is called as variants.

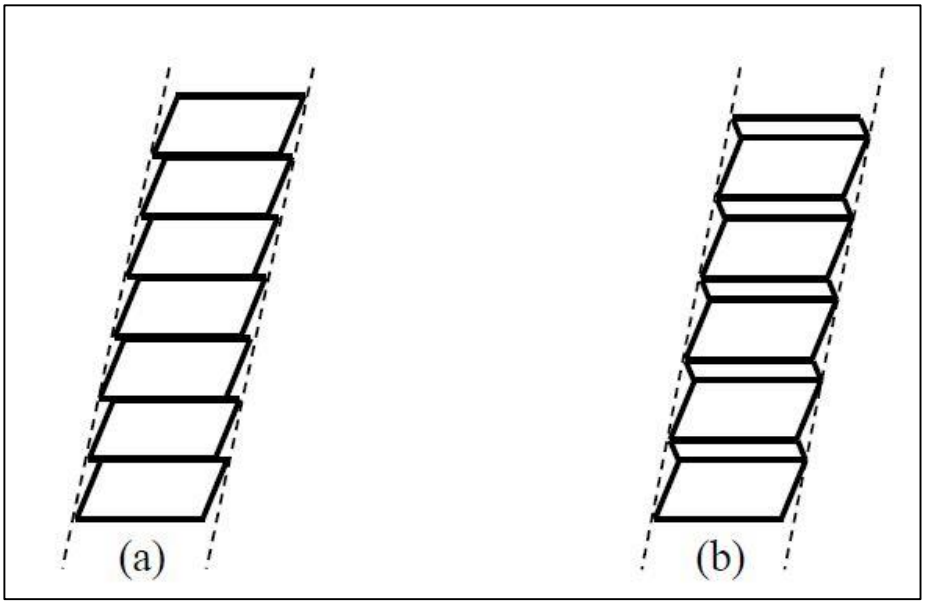

Figure 1.3. Schematic diagram of the two typical basic accommodation mechanisms (a) Internally slipped; (b) Internally twinned [5].

By considering the austenite structure, different martensitic variants are formed in various orientations according to the primary austenite. It gives the possibility of self-housing in their lattice distortions which is 3D configurations for martensite to form structure of specific group by mechanical shape conversion to the phase

transforming matrix, the whole scenario is called the self-accommodation Figure 1.3. There are 24 martensite variants for austenite cubic symmetry which are observed in dual Nitinol. Fig. 1.4 represents the self-accommodation structure for martensite variants which are in Nitinol; (a) Surface relief optical micrograph exposing the self-adjusted martensite of the B19 in an almost equiatomic nitronite [6].

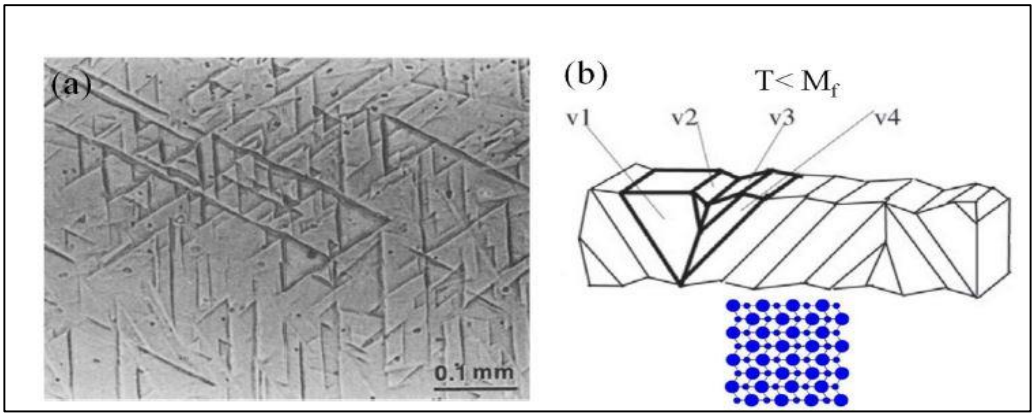

Figure 1.4. The self-accommodation of martensite variants [7].

1.2. THERMOMECHANICAL BEHAVIOR OF MARTENSITIC TRANSFORMATIONS

1.2.1. Thermal Behavior

According to the previous explanation, why it can be tempted for both potential applications of temperature variations and a stress. The tempted temperature for martensitic phase transformation happened at zero load. The martensitic process transition happened due to the shift in the physical and mechanical character. By various detected techniques like electrical resistance measurement, scanning calorimetry, mechanical dilation measurement which is known as thermomechanical analysis and internal friction measurement is also known as dynamic mechanical analysis are used for phase transformation [8].

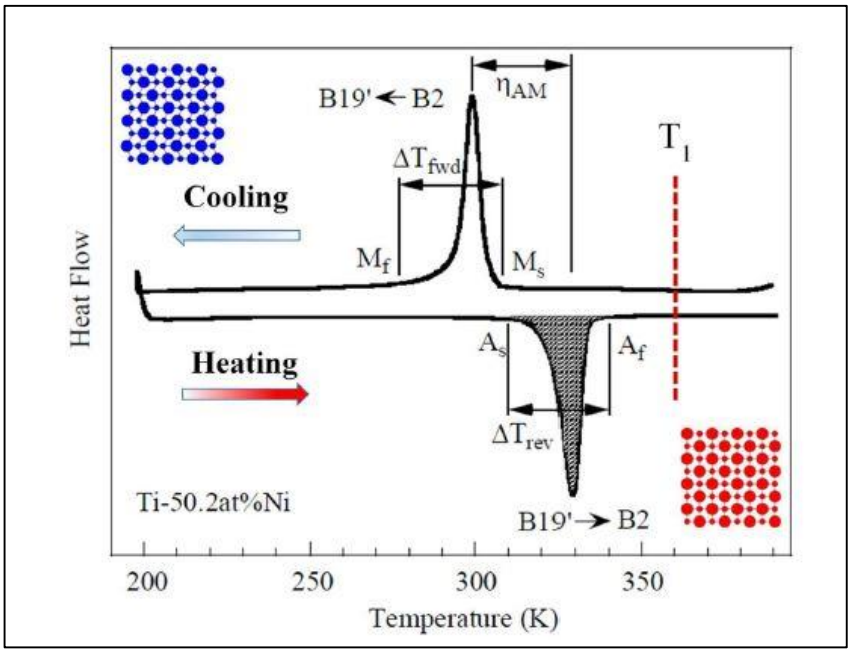

Figure 1.5. Temperature induced martensitic transformation in near equiatomic Nitinol [9].

Figure 1.5 shows the different scanning calorimetry measurements for the Ti-50.2 at% Ni alloys which is martensitic transformation. When cooling happened austenite to martensitic transformation occurred which is forward transformation having limit to a finite temperature time, ΔTfwd. One can easily observe during the temperature interval the volume of the martensitic increase by more cooling the temperature and when further cooling it then the increase in volume fraction ceased which is just like elastic spring pulling [9]. Reverse transformation is the phase shift from martensite to austenite but similar to a forward transformation happens when the sample is heated. These phenomenon and characteristics of two features 1st is when cooling and heating continue then transformation or changes continue, and 2nd is heating transformation and cooling phase transformation are vice versa and it is called thermoelastic transformation. Lattice deformation of variants cancelled internally, and no shape change globally occurred due to self-accommodation in the martensite variants. The temperatures that are at the end are used to calculate the phenomenon of thermoelastic martensitic phase transformation which is as and Mf. which show in Figure 1.5. From the DSC measurement, the following transformation parameters are conventionally defined:

ηAM: Thermal martensite − austenite transformation. Thermal hysteresis of martensite. os Tfwd: forward transition temperature interval.

Bear in mind: reverse transition temperature interval.

i.e.: heat shift as determined by the region covered under the spectral thermal peak during transformation.Mechanical behavior.

A phase shift show various mechanical effects which are depend on ambient temperature. Figure 1.6 elaborates the different distortion effects of near equiatomic of Nitinol at various temperatures. The red lattice represents austenite, the blue square-shaped lattice represents the self-accommodated martensite and the blue parallelogram-shaped lattice represents the oriented martensite. A different scanning calorimetry measurements curves facilitate to depiction of stress-strain effect at various temperature [10]. The distortion effect divided into three types depending upon testing temperature, which includes shape memory effect, pseudo elastic behavior and martensite reorientation [11].

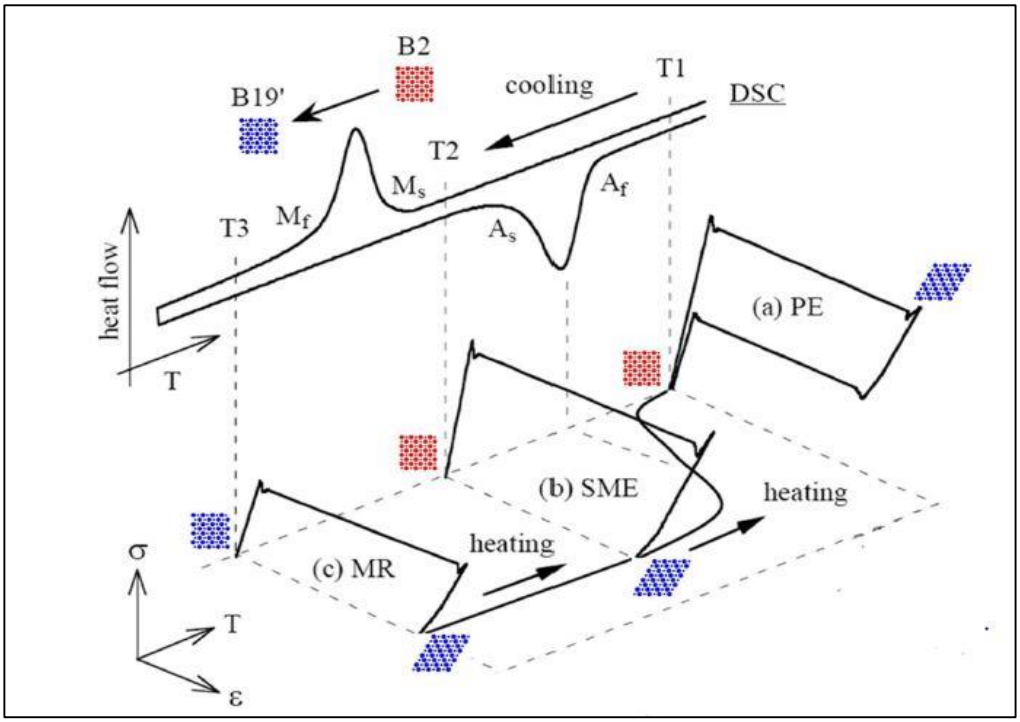

Figure 1.6. Thermomechanical behavior of a near equiatomic Nitinol [11].

1.3. SHAPE MEMORY EFFECT

It is known like “smart material” due the change mechanical stress with temperature. They show the SME which is the phenomenon of restoring the shape or deformed sample; deformed by heating to critical temperature. It is from the thermoelastic martensitic phase transformation. Martensite is happened at lower temperature and can be change its shape easily by de-twinning. And when the phase transformation temperature above the critical temperature then it converts into austenite and restore its original shape [12].

This rotation repeated several times as the crystalline structure is safe. Fig Demonstrates the SME of shape memory alloy wire. The SMA with higher performances can bear up to 8% distortion. Due to the SME these alloys are called as shape memory alloy. It occurs as a result of phase transformation which is described in earlier part. Detwinning arises in the martensite state and seems like a plastic distortion within macroscopic scale due the material stress. And when heating the martensite phase converted into austenite, which is the original phase of the material. And when cooling occurred the austenite phase transforms into martensite phase which is original geometry.

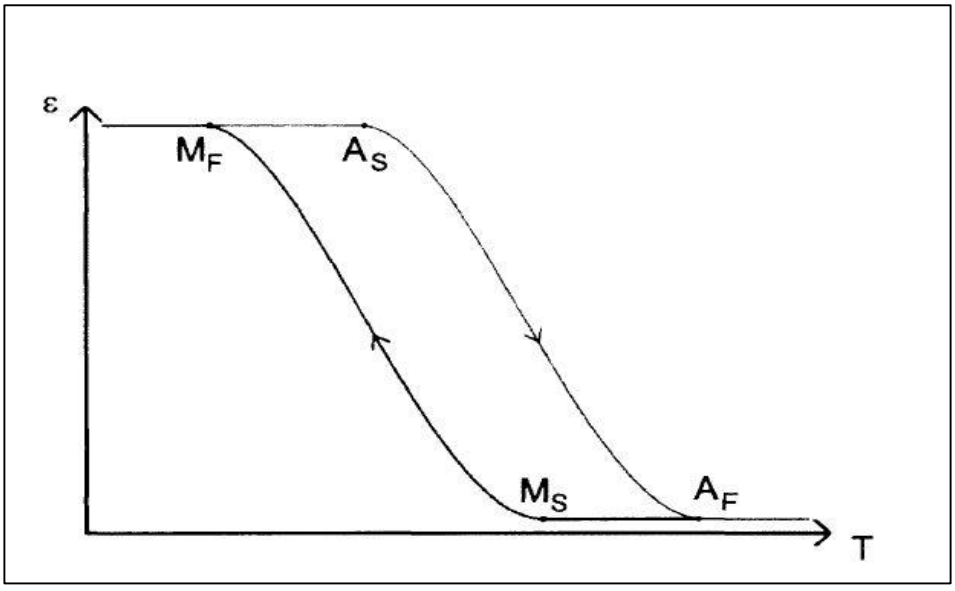

Figure 1.7. Temperature-strain hysteresis during phase transformation of shape memory [13].

Fraction of original phase is determined with temperature and mechanical stress during the phase transformation. Stain depends on temperature applied stress because strain is a function of martensite section. Due to the mechanical stress the critical temperature holds the phase transformation process; ends and start. But the transformation process of reverse and forward phase transform (martensite to austenite and austenite to martensite) is different as its phase transformation temperature is different [14]. Due to this hysteretic behavior appears in Nitinol, it is due to the observation of relationship and properties of martensite section, electrical resistance and strain. Figure 1.7 depicted the temperature and applied strain curve for Nitinol wire within the tensile load. The wire is extended start of the curve due the applied stress. When heating the wire, the temperature rises at critical temperature where the martensite phase transforms into austenite phase transformation this critical temperature is some time known as austenite critical temperature. The phase transformation only occurred when the temperature gradually rises. A_f is the austenite phase transformation at finish critical temperature.

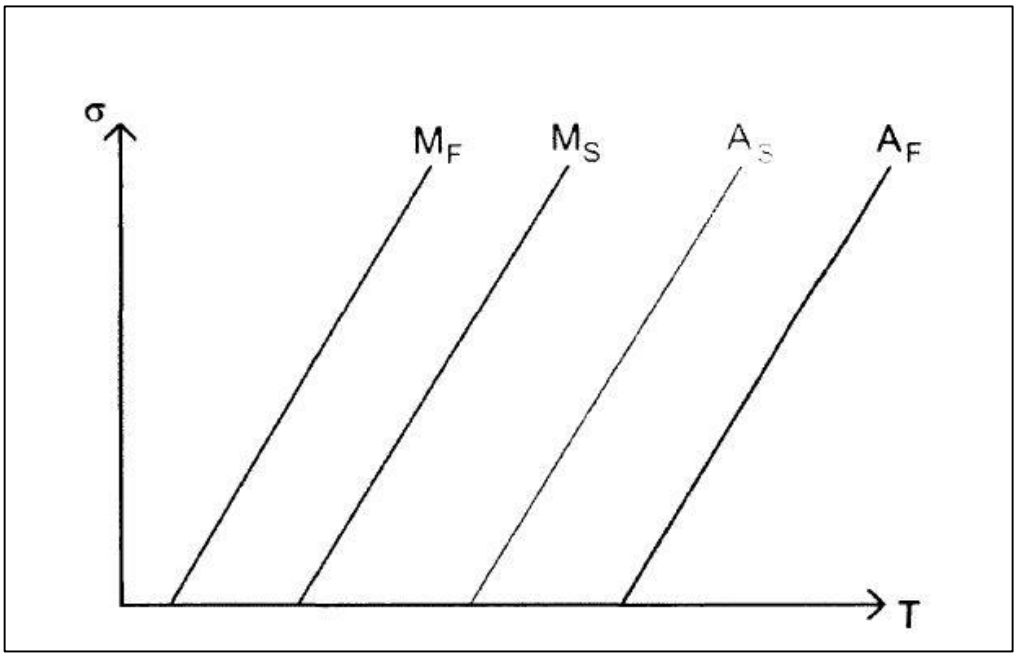

Figure 1.8. Influence of applied stress upon phase transformation temperatures [13].

When the wire or sheet's cooling start then phase transforms when it reaches the critical temperature of martensite phase transformation which is M_s; from austenite to martensite this temperature. As the temperature decreases the austenite to

martensite phase transformation reaches at martensite finish critical temperature M_f. if we did not apply any bias load then then wire attain its original geometry. If the bias load applied, then the wire distorts its state and it allows the material to be used an actuator [15]. By cooling or at low temperature the martensite state detwinned under the bias load and at high temperature the phase transform is recovered. Force and displacement produce by following the stress during the boundary constraints. By increasing the applied stress, the critical transformation achieved, and it is linear relation. As the stress increased the temperature goes to increase and phase transformation occurred. And phase transformation changes by constant temperature but stress varies. When the temperature is high, but stress is constant the material is austenite and the martensite phase achieved by constant temperature and varying the applied stress. This effect is known as super elasticity.

1.4. NITINOL

Nickel-titanium alloys knows as Nitinol has high strength and durability properties due to its behavior it is favorable for SMA, but it is difficult for processing. Nitinol also shows excellent fatigue and protect corrosion. It is also compatible and useful for many biomedical applications. Nitinol is composed of 55% of titanium by changing the weight composite the result can be altered. But the temperature and phase transformation can be changed by selecting the heat action and tertiary alloying as additional elements like chromium, iron and cobalt [16]. The additional copper increases the fatigue life and also decreases the hysteresis effect. But we need to remove the oxygen and carbon because these elements decrease the properties of alloy. While alloy can be formed in many shapes normally sheet or strip and wires fabrication. Austenite and martensite crystal structures for a Nitinol as shown in fig. 1.9. By sputtering micro and Nano elements can form for various applications. Nitinol alloy in the form of wire has many advantages and high surface to volume ration allows wire cool down quickly which is demanding material. Nitinol wire is flexible and use to gain mechanical advantages. Moreover, modeling thermodynamically and mechanically of wire may be a 1D problem and complexity decrease of the model [17].

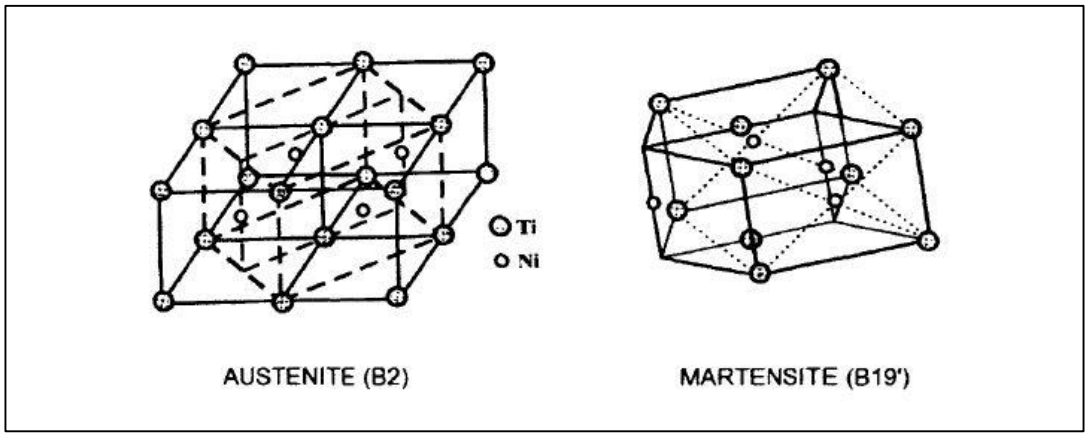

Figure 1.9. Austenite and martensite crystal structures for a Nitinol [18].

1.5. NICKEL-TITANIUM SHAPE MEMORY ALLOYS

The Nitinol is very famous due to its excellent performance and low cost for different applications. Mostly pure stoichiometric Nitinol is composed of 1:1 atomic ratio having 50-50% Nitinol it also presents in 55-45% ration of nickel and titanium with weight percentage. After the discovery of USA, it is known as 55-Nitinol alloy. Otsuka and Ren proposed that 50-50% of Nitinol is the most preferable composition for Nitinol fabrication [19]. To preset the original shape of the alloy temperature used for sintering is about 750-1110°F. Moreover, the deformation of alloy and ability to change phase transformation to its original geometry is depending on sintering temperature. However, the exact sintering temperature is not currently available for fabrication of alloy but varying the temperature Nitinol known as Nitinol is fabricated by using various methods [20].

1.6. PROBLEM STATEMENT

Although Nitinol shape memory alloys have a wide application area, studies on these are limited in our country. This study investigates the application areas, mechanical and metallurgical properties of general sheet metal plates and wires. With this study defining of some material constants will be done such as tensile strength, elasticity modulus, tangent modules and strain hardening index.

1.7. AIM OR GOAL OF THIS WORK

The mechanical and metallurgical properties of nitinol sheet, plates and wires, tensile testing, examination of mechanical properties, internal structure and other memory giving issues are investigated in this work.

1.8. THESIS ORGANIZATION

This work is organized in the six chapters. The aspects covered by each chapter are shown below:

Part 1: Introduction.
Part 2: Literature Review.
Part 3: Theoretical Analysis.
Part 4: Methodology (Experimental Setup).
Part 5: Results and Discussion.
Part 6: Conclusion and Recommendation.

PART 2

LITERATURE REVIEW

2.1. METALLURGY OF NITINOL

In 1963 Buehler discovered the Nitinol based shape memory alloy during the study of heat shielding after the discovery it gains main attention towards shape memory alloy. The main purpose of these alloys is stability and workability which was not seen before the discovery on Nitinol. By melting and casting of materials in a very controlled environment Nitinol based alloys are fabricated in the presence of oxygen which is minimum requirement because Ti reacts with O. The exact and desirable shape of Nitinol samples achieved with rolling, forging, wire drawing, tube extrusion according to the industrial demand and applications. For specific requirements cold working is the only technique to alter the alloy property. To enhance the shape memory properties and applications usage sufficient aging and annealing applied to Ni-rich alloy and Nitinol alloys respectively [21].

2.2. NITINOL BINARY PHASE DIAGRAM AND PRECIPITATION

Below figure depicts Nitinol binary phase diagram. These kind of shape memory alloy are B2 crystal structure and equiatomic composition and we can see in phase diagram. The vertical boundary indicates the B2 phase of Ti side, solubility is not implying of Ti 50% in Nitinol-B2 phase diagram, excess of titanium in the Nitinol alloy. But if Ni can be replaced with Ti in Nitinol-B2 phase about 57% at sintering temperature 1118^0C. Nickel solubility decreases in B2 as the temperature decreases normally about 50% at 630^0C. However, the excess of Ni into Nitinol compound which is shown in binary diagram [22].

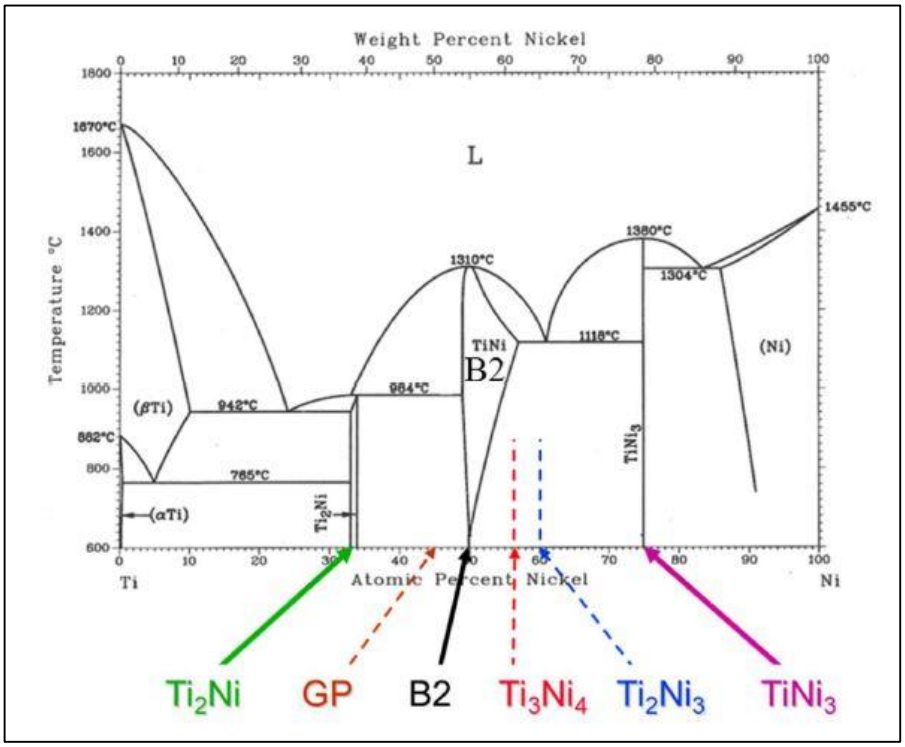

Figure 2.1. Phase diagram of Nitinol system [23].

2.3. DIFFUSIONAL TRANSFORMATION OF NITINOL-B2

At high temperature the Ni-B2 decreases the solubility and implies Nitinol possible precipitation system. These types of diffusional precipitation are confirmed by experiment for both sides as Ti-rich and Ni-rich sides. Ni-rich system of precipitation can be formed in various forms which include TiNi3, Ti2Ni3 and Ti3Ni4. GP zones can be observed on the Ti-rich side and also Ti2Ni precipitation also observed [24]. These are shown in Figure 2.1. Above figure depicts phase transformation diagram of Ti-52% Ni alloy. At shorter ageing and lower temperature, it can be seen that Ti3Ni4 form. TiNi3 phase form only at longer aging and higher temperature and suddenly time and temperature Ti2Ni3 phases originated. $Ti2Ni_3$ concerts to $TiNi_3$ and Ti3Ni4 conversion into Ti2Ni3 during the phase stability of precipitates of Ni-rich with previous Ti3Ni4 and Ti2Ni3. This experiment confirmed that both Ti_2Ni3 and Ti_3Ni_4 phases are in-between phases, the equilibrium phase is TiNi3 and they follow evolution order to increase temperature and increase time as below equation (2.1):

The different Ni-rich precipitates imply different solubilities of Ni in the B2 phase, according to thermodynamic principles. Figure 2.3 shows the experimentally measured solvus for Ti_3Ni_4, and the indicative solvus for Ti_2Ni_3.

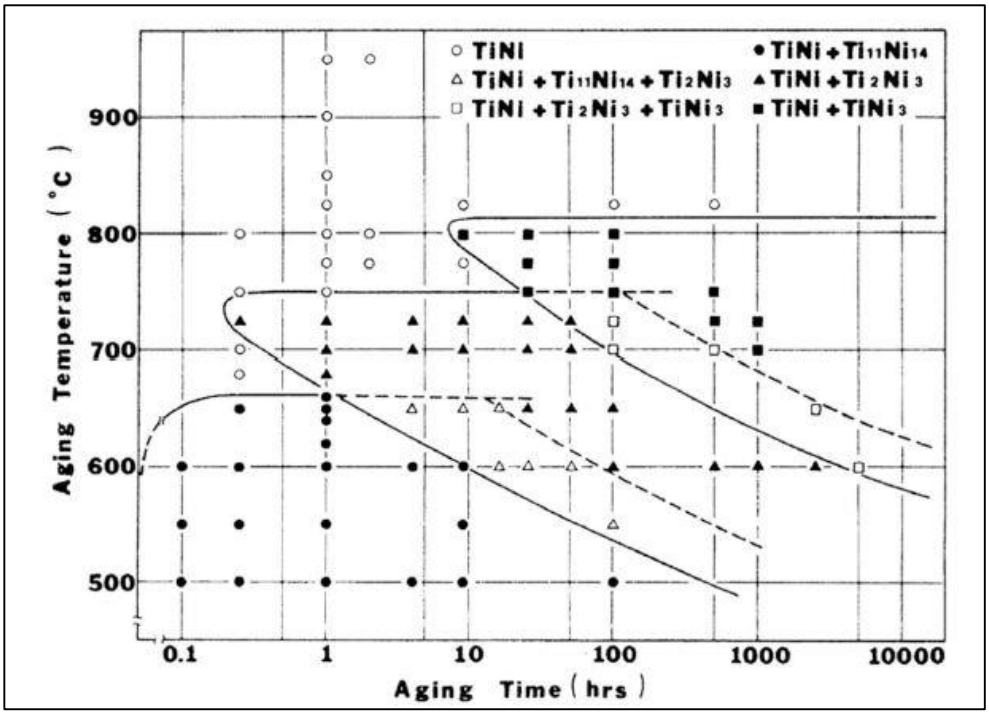

Figure 2.2. Time-temperature-transformation (TTT) diagram of aging behavior for Ti- 52 at% Ni alloy [25].

Among the three Ni-rich precipitates, Ti_3Ni_4 has the strongest influence on phase transformation behavior and properties of alloy due to its crystallographic coherency with the matrix, its small sizes and its dispersed distribution in the matrix. Fig. 2.4(a) shows the microstructure of a Ti-51 at% Ni alloy containing Ti_3Ni_4 precipitate particles. The Ti_3Ni_4 particles are lenticular in shape and are oriented in three variant directions in this case, along the {110} planes of the B2 matrix. Ti_3Ni_4 has a trigonal crystal structure composed of six layers with one additional Ni atom occupying a Ti atom position on every second layer, thus containing 18 Ti atoms and 24 Ni atoms [25]. As a result of the slight lattice gap between matrix and precipitate, there is a strain field within matrix around the precipitate.

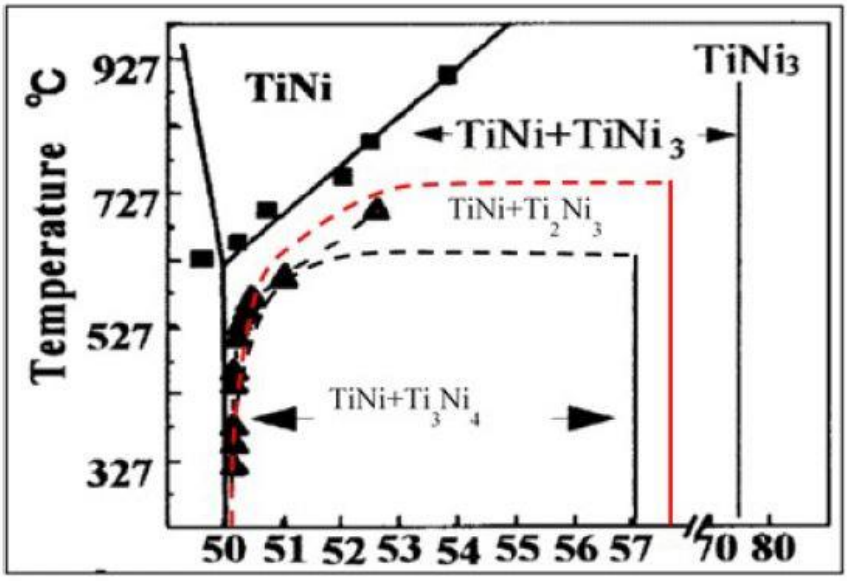

Figure 2.3. Metastable precipitation phase diagram in Ni-rich Ti alloy systems [26].

Figure 2.4 reveals the calculated strain field surrounding a coherent Ti_3Ni_4 precipitate in an austenitic $Ni_{51}Ti_{49}$ matrix. It is clear that there are compressive strains at the edges of the lenticular shaped precipitate particle and tensile strains along the two side surfaces of the precipitate particle. The presence of the stain field is also confirmed in transmission electron microscopy. On the other hand, consequently interface dislocations form to partially relax the strain fields [26,27]. These strain fields play a role in behavior altering the transformation, developing the two ways SME, and inducing B2→R transformation.

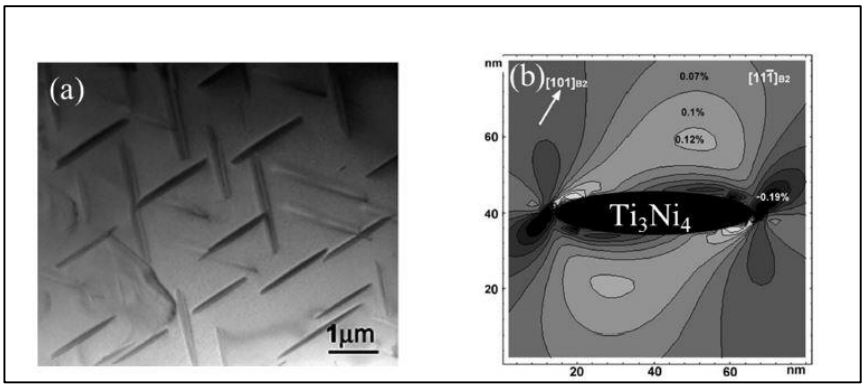

Figure 2.4. Ti3Ni4 precipitates in a Ti-51 at% Ni alloy. (a) Transmission electron microscopy image of lenticular shaped Ti3Ni4 precipitates; (b) Calculated strain field around a Ti3Ni4 precipitate [28,29].

2.4. MARTENSITIC TRANSFORMATIONS OF NITINOL-B2

In addition to the diffusional transformations that occur generally at elevated temperatures, the B2 phase exhibits multiple reversible martensitic transformations upon cooling Figure 2.5 summarizes the possible martensitic transformation routes experimentally observe in Nitinol-X alloys. In case of binary Nitinol, crystal structures observed are three in experiment, consists of a trigonal R phase, a B19′ monoclinic martensite, B2 austenite, which may appear in between the B2 and B19′ phases under certain conditions [3,28].

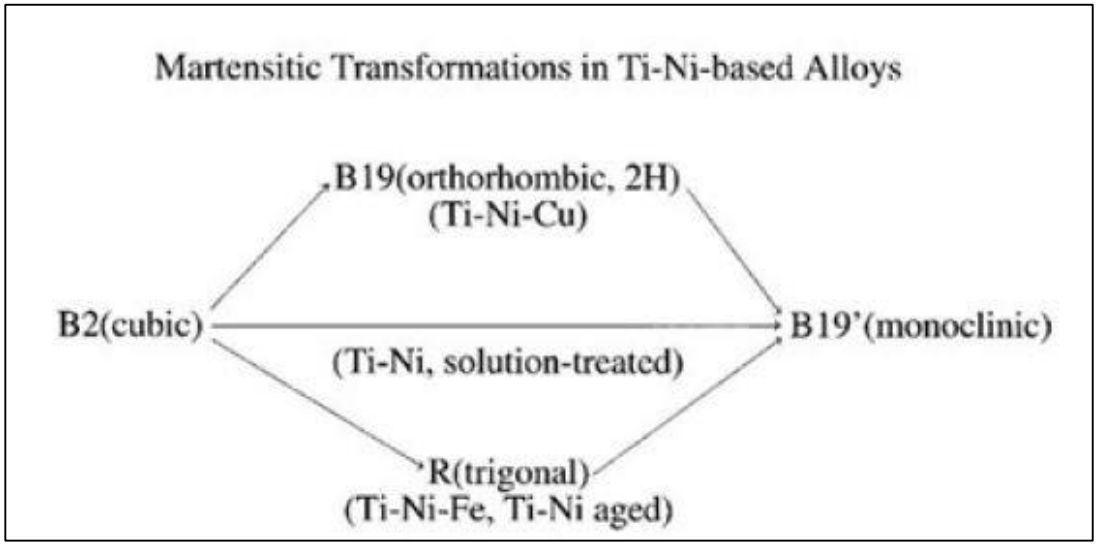

Figure 2.5. Possible experimentally observed martensitic phase transformation paths in Nitinol-X shape memory alloys.

Among the three phases, there are three possible martensitic phase transformations, i.e., B2 to B19′, R to B19, and B2 to R, where B2 is always a paternal phase to R and B19′, and R is parental to B19′. The R phase has been observed in ternary alloy systems, such as NiTiFe, NiTiAl, and NiTiCo. For binary Nitinol, the R phase may appear under certain conditions, such as aged Ni-rich alloys, after thermal transformation cycling [30], or partially annealed after cold working [31]. Figure 2.6 shows the crystal structures of the martensitic phases and the B2 austenite of near equiatomic Nitinol. Also shown for each phase are their [110] projections. Figure 2.6 shows the B2 structure. The B2 phase may also be represented as its equivalent body centered tetragonal (BCT) structure to be comparable to the martensitic phases, as

indicated by the unit cell defined by the red lines. The lattice constant of the B2 structure is 3.015 Å [29,32], which gives the lattice parameters of a = 3.015 Å, b = c = 4.26 Å for the equivalent BCT structure. The BCT unit cell contains 4 atoms, including 2 Ti and 2 Ni atoms.

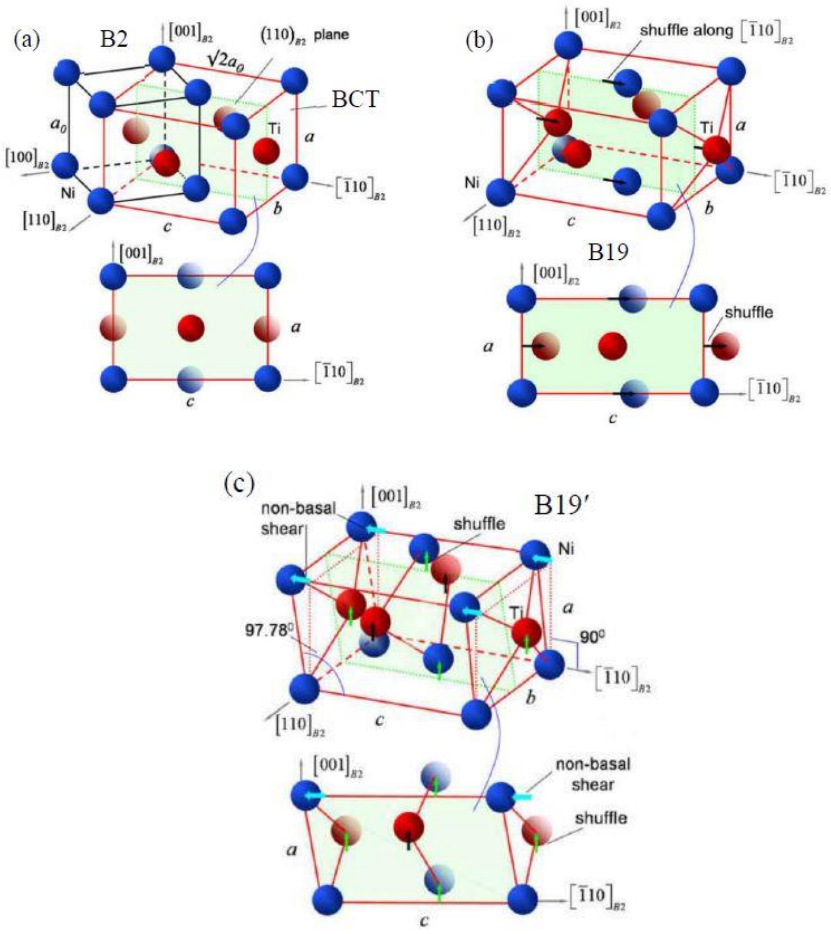

Figure 2.6. Typical phases in NiTi based shape memory alloys: (a) The B2 austenite, which can also be represented by a BCT unit cell; (b) Orthorhombic B19 martensite [33].

The B19 structure is shown in Figure 2.6 (b). It has an orthorhombic structure. It can be formed from the BCT phase by shuffle of the interior Ti and Ni atoms along the [001] B19 direction. This transformation has been reported to be associated with a volumetric contraction [34]. Parameters are a = 2.81 Å, b =4.19 Å, and c = 4.71 Å [35].

The B19′ structure is shown in Fig. 2.6(c). It is a monoclinic structure with a monoclinic angle of 97.8°. The lattice parameters experience a slight change from B19 to B19′. Parameters are a = 2.9 Å, b =4.11 Å, and c = 4.65 Å [36]. The experimentally observed transformation in near-equiatomic Nitinol is the B2↔B19′ transformation. This transformation is hypothesized to follow phenomenologically in two different steps. 1st step is B2 to B19. This phase transformation occurs via lattice volumetric distortion (contraction) and shuffling of the Ni and Ti atoms along the [1] B19 direction, as indicated in Figure 2.6(b).

2.5. EFFECT OF ALLOY COMPOSITION ON THE MARTENSITIC TRANSFORMATIONS OF NITINOL

The transformation behavior and the shape memory properties of phase martensitic transformation near-equiatomic Nitinol are found to be highly sensitive to small variations in its chemical composition. Figure 2.7 indicates the effect of Ni content on the Ms temperature of the B2 → B19′ (A→M) transformation (denoted T_{A-M}) [31]. The T_{A-M} temperature remains unchanged on the Ti- rich side. This is due to the fact that the B2 phase cannot accommodate more Ti above 50.0 at% and the excess of Ti forms into Ti_2Ni, as shown in the Ni-Ti binary phase diagram (Figure 2.1). Consequently, the B2 matrix remains practically equiatomic. On the Ni-rich side, T_{A-M} decreases with increasing Ni content at about 10 K per 0.1 at.% increase of Ni [37]. Also expressed in the figure are the indicative trends of critical temperatures for the A→R transformation (T_{A-R}) and R→M transformation (T_{R-M}).

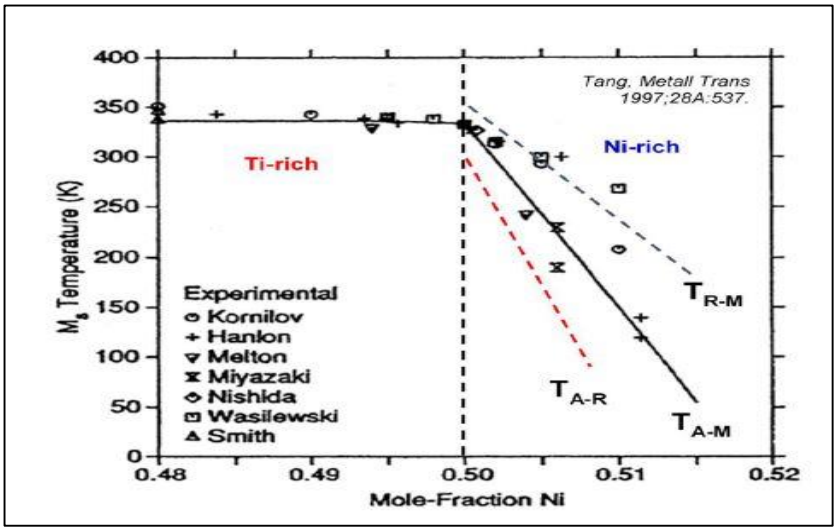

Figure 2.7. Experimental data on the effect of composition variation on the transformation start temperature (Ms) [38].

Addition of some ternary elements has been found to impact on the thermal hysteresis and the transformation temperatures of Nitinol-based shape memory alloys significantly. Generally, adding elements right below Ni or Ti in the Periodic Table increases MS. On the other hand, addition of elements appearing between Ni and Ti in the Periodic Table decreases MS. Cu is found to slightly decrease MS but significantly reduces the thermal hysteresis of the B2-B19′ martensitic transformation [39], [40].Summarizes the effect of ternary alloy addition on the phase transformation temperatures of SMA [41]. Table 1. Effect of ternary alloy addition on the transformation temperatures of shape memory alloys at different conditions [42].

2.6. THERMOMECHANICAL TREATMENT OF NITINOL

The behavior of thermoelastic martensitic phase transformations, thus the properties of Nitinol SMA, can be strongly exaggerated by thermomechanical treatment and also change in the composition of the matrix. Therefore, along with the change of the alloy's composition, different thermal and mechanical treatments have been utilized to alter the shape memory properties of SMAs. In the case of the binary Nitinol, the effective treatments can be separated for near equiatomic Nitinol and Ni-rich alloys (Ni>50.5 at%). The near-equiatomic alloys respond directly to cold working and

annealing. The Ni-rich alloys, due to the B2 phase's solubility for excess of Ni and the change of the solubility with temperature, aging is the most effective way to influence their properties.

2.7. COLD WORKING OF NEAR EQUIATOMIC NITINOL

The cold working decline the B2↔B19′ martensitic phase transformation temperature of near equiatomic Nitinol and persuades the B2↔R transformation, thus changing the transformation sequence from B2↔B19′ to B2↔R↔B19′ (more often B2↔R↔B19′ on cooling and B19′↔B2 on heating) [43]. Meanwhile, the latent temperature of the B2-B19′ martensitic transformations is also reduced. The main reason for these effects is the increased dislocation density and grain refinements. This is generally attributed to the resistive effect of dislocations and to the lattice shape change of the martensitic transformation. Therefore, the B2↔B19′ transformation is much more affected (retarded) by the increase of dislocation density in the matrix than is the B2↔R transformation, because of the much larger lattice distortion of the former. Following the same argument, thermal transformation cycling has also been observed to have the similar effect, because it can be considered a very mild repeated process of gentle plastic deformation of the matrix [44]. Severe plastic deformation, however, will destroy all the martensitic transformation in the alloy. Such cold deformation is most commonly applied as a material working process than a transformation behavior control process and is often used in conjunction with post deformation annealing.

2.8. EFFECT OF ANNEALING ON TRANSFORMATION BEHAVIOR OF NITINOL

Annealing of near equiatomic Nitinol after severe plastic deformation restores the transformation behavior of the alloy. Fig. 2.8 shows the consequence of annealing on the phase transformation temperatures of a Ti-50.2 at. % Ni alloy. The transformation behavior can be divided into three regions. For region I at below 700 K, the B↔R transformation is restored, apparently due to its small lattice distortion and thus the least mechanical resistance in a heavily defected matrix. Rf increased

with increasing the annealing temperatures leading to lower transformation intervals in region I. In region II, R↔B19′ transformation became evident. The M_f and M_s Temperatures enlarged quickly with increasing the annealing. Finally, for the high annealing region, the transformation sequence was B2↔ B19′ and independent of annealing.

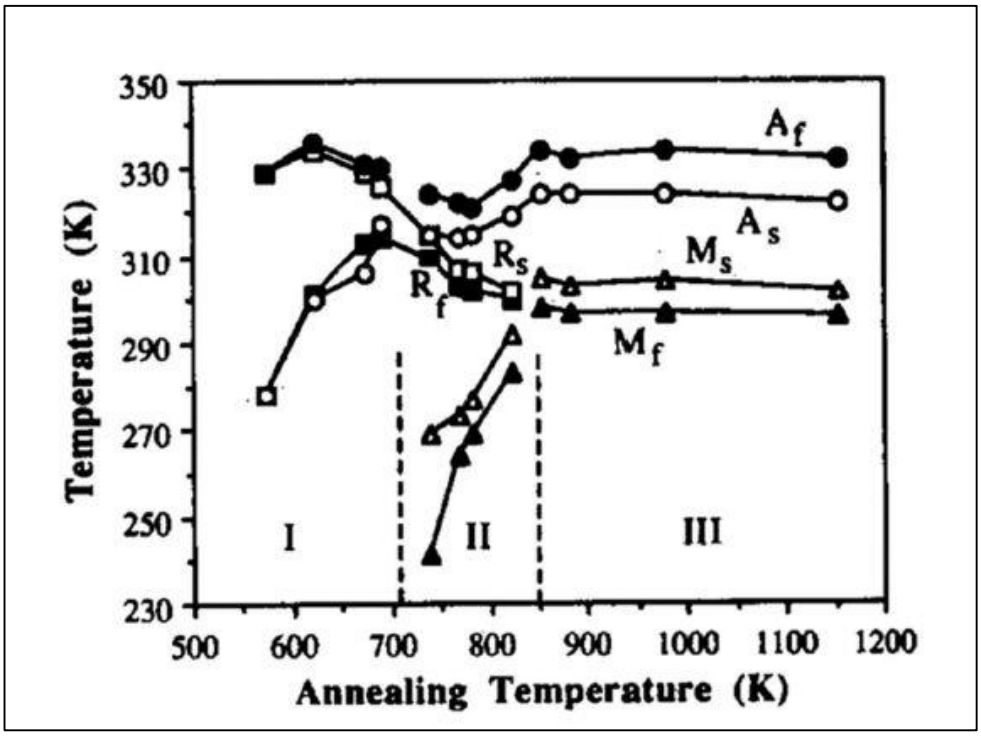

Figure 2.8. Transformation temperatures of annealed near equiatomic Nitinol at different temperatures for 30 min measured by DSC [45].

2.9. EFFECT OF ANNEALING ON MECHANICAL BEHAVIOR OF NITINOL

Annealing after cold working has been found to progressively restore the mechanical behavior of near-equiatomic Nitinol, including the stress-induced martensitic transformation and pseudo elasticity. Fig 2.9 shows the strength dependence of Nitinol upon different annealing temperatures. Figure 2.9 indicates distinctive tensile stress and strain curves of a Ti-Ni 50.2 at% sample at three temperatures after annealing at 776 K. It is seen that the sample has recovered its mechanical behavior after severe plastic deformation. A summary of the effect of annealing after cooling on the yield

strength and stress for persuading the phase transformation in a Ti - 50.2at%Ni alloy is shown in Figure 2.9(b) [46]. The alloy is found to exhibit super elasticity after annealing at 660 K for 1.8 ks. At above the recrystallization temperature, the alloy exhibits shape memory behavior. It is also seen that the yield strength, stresses for stress- induced phase transformation at a given testing temperature and for martensite reorientation increase gradually with growing annealing in this range. The increase of those parameters is not explained explicitly in the literature, but is supposed to be connected to surface oxidation of the alloy when annealed in air.

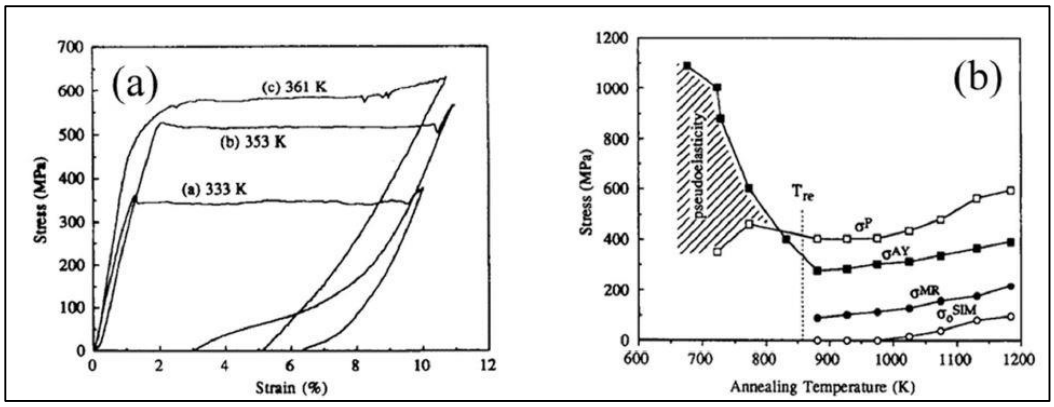

Figure 2.9. Strength dependence of NiTi upon different annealing temperatures. (a) Typical stress-strain behaviour of a Ti-Ni 50.2 at.% sample annealed at 776 K and tested at different temperatures; (b) Strength vs annealing temperature for a Ti-Ni 50.2 at.% sampl.

2.10. AGEING OF NI-RICH NITINOL

In comparison to the near-equiatomic (typically Ni > 50.2 at %) alloys, the Ni-rich (typically with Ni > 50.5 at %) alloys have much more complex response to heat treatment. In addition to annealing, they also exhibit sensitive response to ageing. Aging treatment can be applied to Ni-rich alloys to promote the nucleation and growth of Ni-rich precipitates [48]. Alloys with lower Ni contents have also been found to precipitate Ni_4Ti_3, but it generally requires longer aging times. The temperature range for aging is generally 450-750 K [49]. Ti_3Ni_4 is the first precipitate to form upon ageing. Figure 2.10 shows Ni_4Ti_3 precipitation in a Ni-rich Ti sample [50].

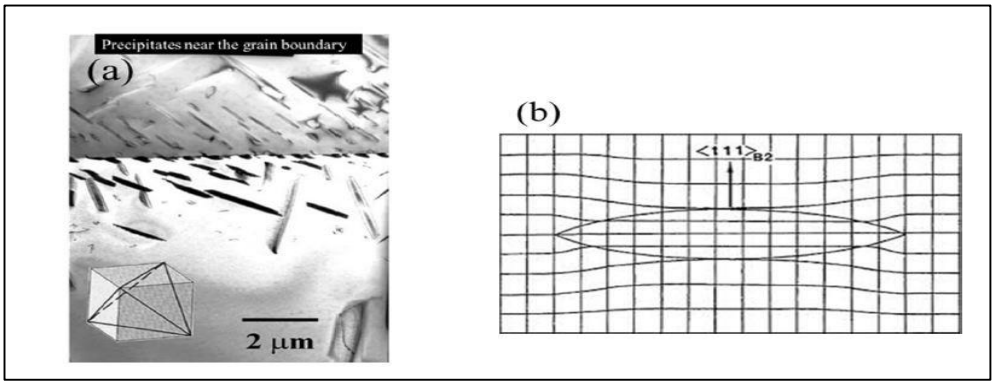

Figure 2.10. Ni4Ti3 precipitation in a Ni-rich Ti sample. (a) TEM image of formation of precipitates near the grain boundary after aging of Ni 50.7 at%-Ti alloy for 1 hour at 500^0C; (b) Schematic of coherency between Ni4Ti3 and the B2 phase of the matrix in age [51].

Figure 2.10 indicates a TEM image of formation of precipitates near the grain boundary after aging of Ni 50.7 at%-Ti alloy for 1 hour at 500^0C [33]. Ti3Ni4 precipitates are found to nucleate preferentially at grain boundaries. Figure 2.10 shows the schematic of coherency between Ni4Ti3 and the B2 phase of the matrix in aged Ni-rich Ti alloys. The coherency between the phases leads to formation of Ni4Ti3 in three specific orientations within the matrix. The presence of coherent Ni4Ti3 precipitates in the matrix has significant influence on the phase transformation mechanical properties behavior of Nitinol. The transformation sequence shows different transformation sequences of a Ti–50.9 at.% Ni alloy after different heat treatments. Curve (a) is the solution treatment condition achieved by annealing treatment. This heat treatment condition results in a simple A↔M transformation. Curve (b) proves the transformation behavior of a sample aged at 748 K for 36 ks. On cooling, it exhibits a phase transformation sequence of A→R→M and on heating from M, M→A. Dashed line is the anticipated direct A→M phase transformation, which is forbidden in this case by the occurrence of the A→R transformation. A phase transformation arrangement of A↔R→M can be seen in curve (c), where the sample has been aged treated at 573 K for 3600 ks.

The transformation behavior of Ni-rich alloys has also found to be more complex under certain sample processing conditions. Such behavior is usually observed in samples after aging at low temperatures and shorter times for Ni-rich alloys with less

than ~51at%Ni [52]. An example is for a $Ni_{50.8}Ti_{49.2}$ alloy later aging at 450 °C. It can be predicted that the 1st peak on cooling is A→R phase transformation, and the following peaks represent the creation of B19′, thus R→ B19′. After the third cooling peak, the majority of the R phase has been transformed to B19′, and with further cooling to -100 ^{0}C the amount of the R phase becomes negligible. On heating from a low temperature, the transformation sequence is B19′→R followed by R→ B2. At 80 ^{0}C, the matrix becomes fully B2.

Allafi et al. suggested an explanation about the multistage phase transformation detected in old Ni-rich alloys [38], on the basis of long range heterogeneous distribution of Ti_3Ni_4 precipitates within the matrix. In the initial stages of aging, Ti_3Ni_4 hastens are distributed more specially along with boundaries and much less in the inner of grains, effectively division the matrix in two districts of different phase transformation characteristics, thus the multiple-stage transformation behavior. The 5 stages may be identified for the morphology evolution of Ni_4Ti_3 precipitates during aging, including (I) suppression of B2↔B19′ due to the atomic arrangement heterogeneity; (II) B2↔R transformation; (III) B2↔R↔B19′ transformation sequence after well distribution of the coherent precipitates; (IV) multi stage phase transformation as a result of over-growth of coherent precipitates; (V) B2↔B19′ phase transformation in the presence of non-influential incoherent precipitates. The other influence of the coherent precipitation is the change of mechanical behavior of Ni-rich alloys. Precipitation hardening is a known effect that the yield strength [52]. An example for precipitation hardening in the case of a Ti–50.9 at.% Ni alloy aged at different temperatures for 3.6 Ks is presented in Figure 2.11.

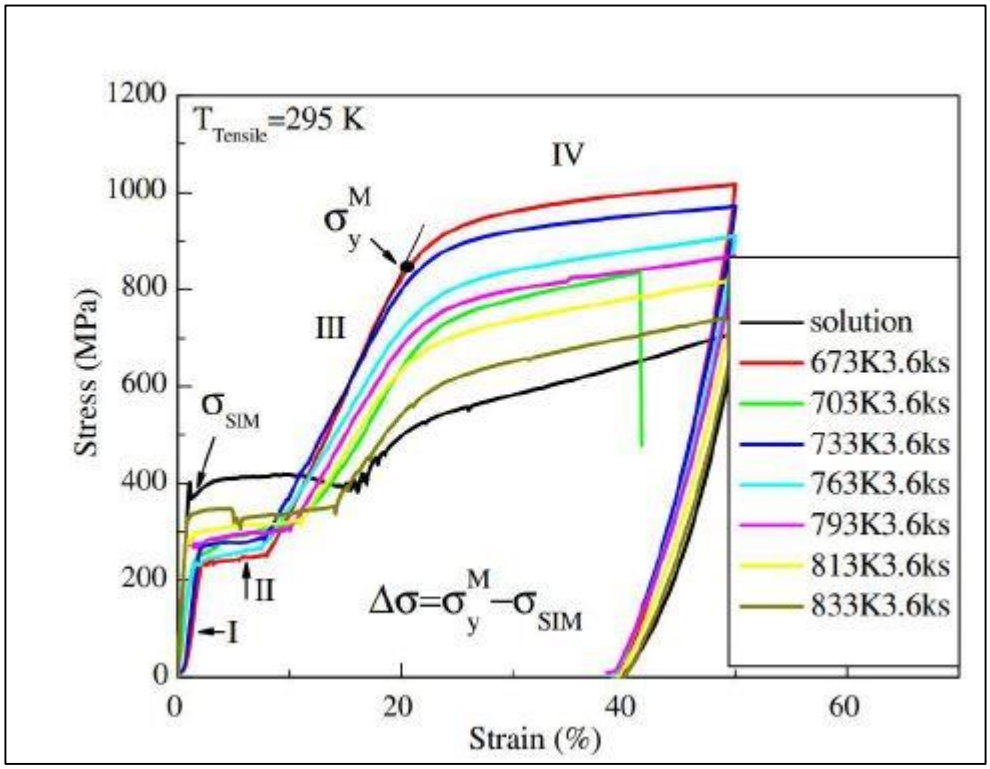

Figure 2.11. Stress-strain response of a Ti–50.9 at.% Ni alloy aged at different temperatures for 3.6 ks [53].

Figure 2.11 reveals the temperature effect on the stress-strain response of the alloy, measured at 295 K [52]. The first obvious result is the starting structure of the samples at stage I as indicated in the figure. The second conclusion is the samples with lower critical stresses showed higher yield stresses and the highest yield stress was for the lowest aged temperature. The solution preserved sample had the last return stress.

2.11. OXIDATION

Oxidation of Nitinol system is usually not a major concern in manufacturing of these alloys for general purposes. However, for miniaturized applications and MEMS devices, where shape memory alloys are used to fabricate components of very small dimensions, surface oxidation can have significant impact to the transformation behavior and mechanical properties of the martensitic transformations [38,54]. The cross section of the annealed sample revealing the Ti oxide and Ni-rich Ti layers. It is known that Ti has a very high affinity to oxygen to form into TiO_2. A surface

oxidation layer can influence the SMP in two apparent details: (i) The surface TiO_2 layer is brittle and functions as a mechanical resistance to shape memory distortion and recovery; (ii) the Ni-rich layers (including $TiNi_3$ and a Ti-depleted zone inside the matrix) underneath the surface oxide are unable to exhibit martensitic transformation, thus hindering the shape memory properties.

Despite the undesirable effects of oxidation on the shape memory properties, in biomedical applications, formation of a thin layer of TiO_2 has been proposed as a technique to shield the Ni leach into bio-systems [55]. It is known that lower Ni interaction with bio-systems at the alloy surface due to formation of TiO2, reduces thrombogenicity [42]. However, several studies have reported that significant concentrations of Ni, ranging from 3 at% to 20 at%, can still be released at through the oxide layer, challenging the technique [54]. Undisz et al. [56] reported that the history of annealing determines the final Ni concentration at the oxide surface and that high heating rates reduce Ni release through the oxide. Another challenge is the surface roughness of the oxidation treated samples for biocompatibility. The SEM results reveal the consequence of annealing on the surface characteristics. The surface is smooth and includes two distinctive components: (1) dark islands with a structure near to TiO ($Ti_{0.55}O_{0.45}$), and (2) a grey oxide layer that has a composition of $Ni_{0.46}O_{0.23}Ti_{0.31}$ [50]. Fig. indicates the surface of a sample annealed at 600□C. Increase the annealing at 600C changed the topography of the surface and made it rougher and grainier. The surface is found to contain mainly Ti and O, and a low concentration of Ni. At 800°C the surface has a dominant porous structure and the composition was measured to be TiO_2 stoichiometry [50].

Natural oxidation of the surface can also change the phase transformation temperatures of Nitinol alloys and essentials to be occupied into account in the design of Nitinol based micro-electro- mechanical systems (MEMS) devices [29]. Li et al. [38] used an in situ TEM setup to investigate the natural oxidation of TEM samples with different thicknesses. They confirmed the oxygen content in the samples and found that the thickness of the TEM sample is a key factor on the thermally induced martensitic phase transformation. They reported that there are critical values 0f ~22 nm and ~50 nm for B2→R and R→B19′ thermally induced

phase transformation, respectively. They attributed the observed size effect to the natural oxidation of Nitinol.

2.12. NEW DEVELOPMENTS OF NITINOL SMA

With the establishment of the knowledge framework for Nitinol SMA, including the fundamental science of thermoelastic martensitic transformations [45], the physical metallurgy of the system [6], the thermomechanical behavior of the alloys [6,32], and the industrial production and processing techniques of these alloys [6,47], new effort has been made in recent years to develop more advanced Nitinol based materials in non-conventional forms and structures to further expand their property capabilities to meet the demands and challenges of more and new innovative applications, such as in microelectromechanical systems (MEMS), bionic and robotic technologies, space science, and mining and resource exploration.

2.13. FUNCTIONALLY GRADED NITINOL

Functionally graded Nitinol alloys allow them to display their functional properties in a progressive and gradient manner. These materials often exhibit progressively varying transformation stresses and transformation temperatures within the body of the material. The widened stress and temperature windows render the alloys better controllability in sensing and actuation applications. The sequential occurrence of the transformation across the body of a material often triggers complex and new mechanical behavior of the materials. Nitinol alloys are known to exhibit Lüders-type deformation behavior upon loading [57,58] A Lüders-type deformation is a mechanical instability with a nil stress window, which gives very poor controllability of the alloy in actuating applications [51]. Thermally induced phase transformations in Nitinol typically have transformation temperature window of about 10 K, which is also narrow and difficult for easy and reliable actuation control. For better actuation controllability, wider transformation stress and temperature windows are desired. Figure 2.12 shows the comparison between the actual and desired behaviors of Nitinol SMA, as in the case of stress-induced transformation in pseudo elasticity (Figure 2.12(a)) and thermally induced transformation (Figure 2.12(b)). One possible

way to achieve such desired thermomechanical behaviors is to design functionally classified alloys.

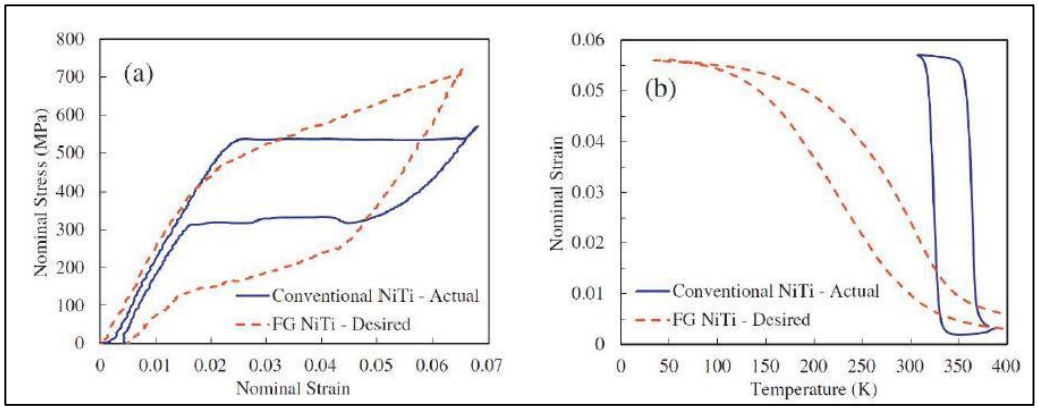

Figure 2.12. Actual behavior of NiTi vs desired behavior of NiTi shape memory alloys. (a) Stress induced phase transformation in superelasticity; (b) Thermally induced phase transformation under constrained condition [59,60].

Nitinol SMA with graded properties can be designed in three different ways: compositional incline, microstructural grade and geometrical gradient. In addition, the property gradient may also be perpendicular or parallel to the loading direction, referred to as the parallel and series configurations, respectively [61,62].

2.14. COMPOSITIONAL GRADIENT

The properties of Nitinol alloys are sensitive to their compositions, e.g., with the addition of a third element [26,63,64] or variation from the Ti-Ni equiatomic stoichiometry [29]. Several different ways are possible to create the compositional gradients in Nitinol, and these gradients may be along the length, such as wires, or through the width, such as thin films and sheets [53,65]. Figure 2.13 shows a compositionally graded Nitinol plate prepared by diffusion annealing. Figure 2.13 indicates the stress –strain tensile distortion samples annealed at different timing and a solution-treated sample. From the figure it can be seen that, the diffusion annealing of Ni into the substrate altered the stress-strain response of the sample. Figure 2.13(d) shows the phase transformation behavior of the similar samples as Figure 2.13(c). The phase change behavior of the annealed samples was changed, and the

second sample shows a continuous forward and reverse transformation (not a sharp peak) probably due to the created compositional variation in the Nitinol substrate.

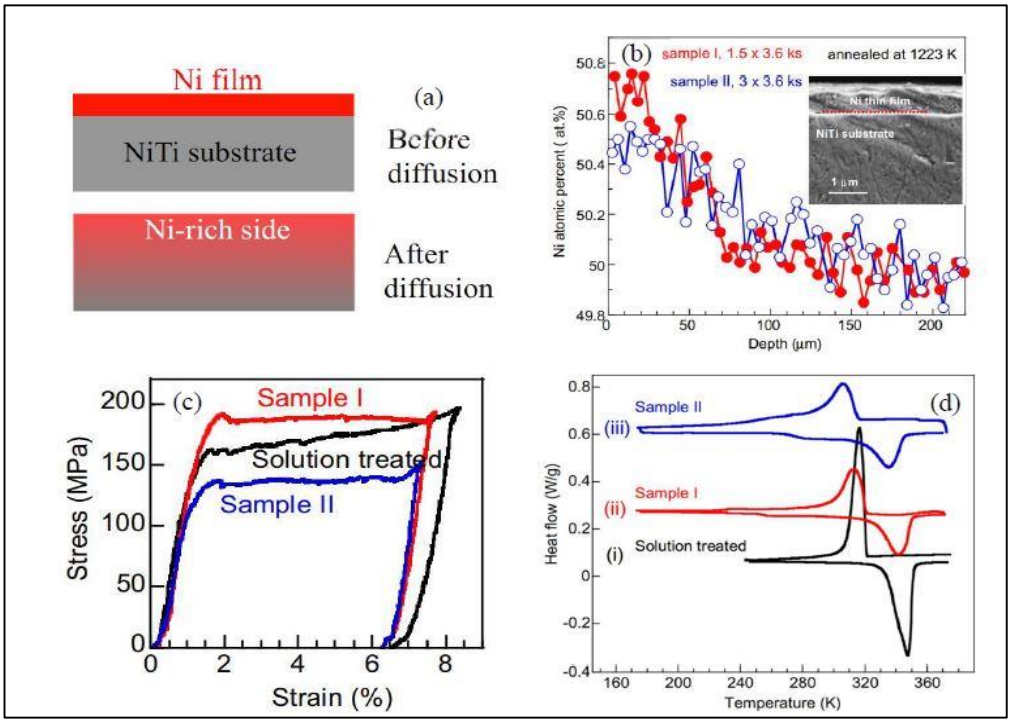

Figure 2.13. Compositionally graded NiTi plate created by diffusion annealing concept. A compositionally graded NiTi plate created by diffusion annealing concept. (a) schematic of the technique; (b) effect of diffusion time variation on Ni concentration variation measured by EDS technique (the inset is a SEM micrograph of the deposited Ni thin film on top of the NiTi substrate); (c) the tensile stress–strain curves of deformation of the two samples annealed at different timing and a solution- treated sample; (d) Transformation behavior of near equiatomic substrate (i) solution treated at 1123 K for 3.6 ks, and diffusion annealed at 1223 K after deposition of Ni for (ii) 1.5 3.6 ks (sample I) and (iii) 3 3.6 ks (sample II), respectively [66].

2.15. MICROSTRUCTURAL GRADIENT

It is known that the phase transformation behavior and the shape memory properties of Nitinol alloys are sensitive to microstructural conditions [67,68], thus concept gradient of functional properties can be attained by creating a micro-structural gradient. The microstructural gradient can be of a cold worked microstructure, annealed microstructure or aged microstructure. Figure 2.14 shows a technique using heat treatment temperature variation to create microstructural functionally graded

near-equiatomic Nitinol SMA [69]. Figure 2.14(a) shows the schematic of the technique. The wire can be subjected to an annealing temperature variation (1) and also differential aging condition (2) created by the non-uniform furnace temperature profile. Figure 2.14(b) shows the stress-strain behavior of a Ti-50.2at%Ni Nitinol sample uniformly galvanized at 773K and then tested at 318K. The curve shows a typical Lüders like tensile deformation. Figure 2.14(c) shows the actual furnace profile used to create the microstructural gradient and the position of the annealed wire in the furnace. Figure 2.14(d) indicates the stress-strain retort of the non-uniform annealed sample. The gradient anneal is measured to be in the range of 550K to 760K. The curve reveals that by non-uniform annealing of the sample, different mechanical properties relative to the uniformly annealed sample can be achieved.

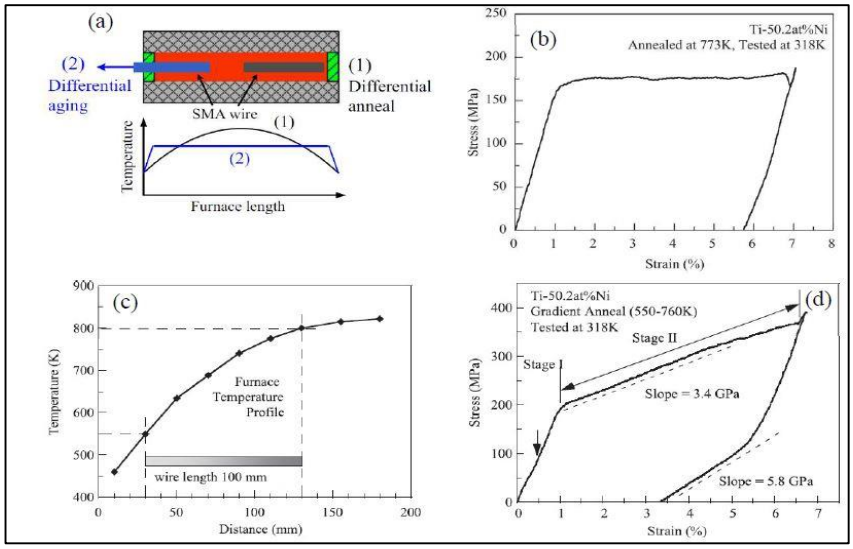

Figure 2.14. A heat treatment method for the creation of functionally graded microstructure [70].

2.16. GEOMETRICAL GRADIENT

The variation of the cross-section area in the direction of the applied load is the key for achieving the geometrical gradient designs. When the loading is applied, the martensitic transformation starts from the lowest cross-section area (i.e. highest stress concentration) and propagates to the highest cross-section area that creates a non-uniform transformation response in the sample. This effect generates an unmatched stress-strain response from the sample with uniform design that can be managed to

create a positive slope can tackle the mechanical instability of SMAs created by lüders bands [71]. Figure 2.15 shows the series and non-series examples.

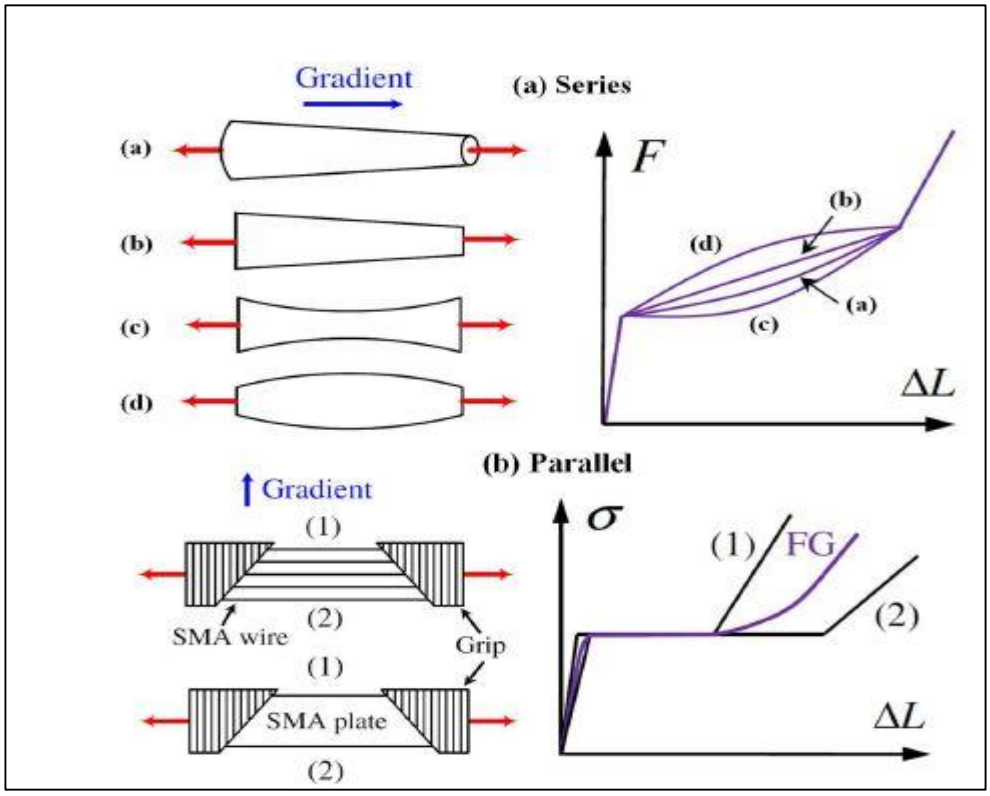

Figure 2.15. Typical microstructural based functionally graded designs. (a) Series configuration; (b) Non-series configuration [59].

2.17. ARCHITECTURED SMAS

The functional properties of Nitinol SMAs can also be combined with the materials geometrical characteristics to offer new and enhanced application performances. Design of the materials to enhance their functionality is not a new concept. For example, I-beams and the tubular framework of bicycles are a well-known examples for enhanced bending stiffness and reduced weight. Another example is helical springs, which trades material stiffness for flexibility and recoverable deflections. Considering these already established concepts, various attempts have been made to create Architectured Nitinol materials for new and better performances, such as springs, cellular designs, network structures and porous design.

A simple architectured design of Nitinol is Nitinol springs. Spring design allows enlarging the recoverable elastic deformation by 1~2 orders of magnitude at the expense of strength. Thus, Nitinol springs are designed when excessively large displacement is required. They are used mainly for storing elastic energy, delivering constant force, and damping vibration [72]. Figure 2.15 shows the application of Nitinol springs in dentistry for space closure, tooth retraction and distal movement [73]. SMA cellular structures can be designed to achieve both low stiffness and high stiffness to mass ratio. The low stiffness designs can be considered as 3D springs and offer the advantage of adjustable stiffness for different application demands. One example is in biomedical applications as bone replacement with matching stiffness (typically 20 GPa) to avoid stress shielding effect [74]. Figure 2.15 shows cellular design of spot-welded Nitinol tubes and its deformation behavior under uniaxial compression [75]. The maximum 12% global compressive strain at three different testing temperatures without damage to the welding could be achieved. The structure exhibited an effective structure elastic modulus of ~25 GPa, which is very close to the reported modulus for bone.

Figure 2.15 shows another example of Nitinol cellular structure in honeycomb design and its deformation behavior under uniaxial compression [76]. The structure exhibited 60% pseudoelastic deformation and an apparent effective elastic modulus of 19.1 MPa. Another architectured design is network structures. They can be fabricated by weaving, braiding, knitting and stitching Nitinol wires and strips in 2D or 3D designs [77,78]. The designed geometrical network can be controlled to reduce the stiffness and produce a large recoverable deformations unmatched with the monolithic binary Nitinol. A typical example of network designs is woven Nitinol stents. Nitinol stents are capable of being compressed into a catheter in much reduced size and self-expanding against the vessel’s wall once deployed inside the body owing to its shape memory super elasticity. It illustrates a self-expanding Nitinol stent released from a catheter and an endoscopic view inside a self-expanded stent after insertion.

2.18. DEVELOPMENT OF THEORETICAL UNDERSTANDING OF NITINOL

However, with the development of density functional theories and computation tools in the past decade, many studies have been conducted on Nitinol system to discover some new phases that have never been observed experimentally and challenge the experimentally reported B2 phase. The DFT method has also allowed identification of transformation pathways between different phases, determination of the ground state, and investigation of stabilities of various phases. One worth mentioning discovery using the DFT method is instability of the B2 austenite phase, while the B2 phase is observed frequently in experiments. The other such findings is the discovery of the B19″ phase and a base centered orthogonal (BCO) phase in the binary near-equiatomic Ni-Ti system, which demonstrate a clear discrepancy with experimental observations.

2.19. THERMAL STABILITY OF THE B2 PHASE IN EQUIATOMIC NITINOL

The equiatomic Nitinol exhibits a B2 austenite phase of CsCl-type structure in $Pm\bar{3}m$ space group (no. 260) with a lattice constant of a=3.015 Å [30]. The dynamic stability of the phase may be examined using the frozen phonon technique. It displays the phonon dispersion of the B2 phase at 0 K based on the forces extracted from DFT calculations and used in the frozen phonon approach. For further comprehension about the entropic effects on B2 phase, researchers have attempted to combine the DFT calculations at 0 K, where there is no entropic effect, with other methods such as the self-consistent ab initio lattice dynamical (SCAILD) calculations and the ab initio molecular dynamics (AIMD). Zarkevich and Johnson used AIMD method to add the entropic effect to the B2 phase. They used a 3×3×3 supercell with 54 atoms [79]. They found that the B2 structure is thermodynamically unstable at all temperatures up to its melting temperature, 1586 K. This conclusion clearly contradicts the reality and could be attributed to the size of the supercell used. They proposed a new crystal structure for the B2 phase to solve this puzzle [80]. In contrast, Souvatzis et al. by using first principles SCAILD calculations method

confirmed that the B2 phase in equiatomic Nitinol is stabilized by phonon-phonon interactions [81]. Recently, Haskins et al. revealed the importance of the size effect of the supercell when AIMD method is used. They also reported that the imaginary (negative) frequencies of phonon dispersion become positive (stable structure) at 300 K, which is very close to the experimentally reported temperature for the B2↔B19′ transformation. Figure 2.34 shows phonon dispersions at 600 K for 3 different supercell sizes as calculated by Haskins et al. [59].

2.20. THE GROUND STATE OF EQUIATOMIC NITINOL PREDICTED BY DFT CALCULATIONS

In ternary Nitinol based shape memory alloys, such as NiTiFe, NiTiAl, and NiTiCo, the B2↔R transformation is known to occur spontaneously [66]. B19 is another experimentally observed phase in NiTiCu alloys with an orthorhombic crystal structure. It occurs in $Ni_{50-x}Ti_{50}Cu_x$ alloys when the Cu content exceeds 7.5 at.% [82,83]. Table 2.2 presents the lattice parameters, monoclinic angles, and the energy differences of the theoretically predicted phases with respect to the B2 parent phase. The BCO phase was first reported by Huang et al. [3]. In their DFT calculation, the monoclinic angle of the martensite corresponding to the minimum energy distortion is found to be 107°, and not the experimentally reported 98° for B19'. They identified this as a new phase with BCO structure and confirmed that it is effectively also a monoclinic phase similar to B19′.

To gain more insight about the BCO phase, Huang et al. constructed a minimum energy pathway (MEP) against monoclinic angle within the range from 90^0 to 112^0 [3]. They also considered PdTi and PtTi, which are known to also have monoclinic martensite, for comparisons with NiTi. Fig. 2.35 shows the MEPs as a result of the monoclinic angle change for NiTi, PdTi and PtTi alloy systems. The calculations revealed that there is a local minimum representing the B19′ martensite at ~93^0 angle in the PdTi and PtTi systems, whereas for the Nitinol system a local minimum occurs at around 107 representing the BCO phase. There is no local minimum at the experimentally observed monoclinic angle of 97.8′ for B19′ phase. This analysis confirms their early calculation that BCO is the ground based on the structure

optimization technique. This finding that the BCO is the ground state instead of B19′ contradicts the common experimental observations and imposes a question to the existing knowledge of binary Nitinol. After stablishing the BCO phase as the local minimum instead of B19′, and to attempt to answer the question why B19′ is experimentally observed, they applied a shear stress to the B19′ and found that a shear stress within the range between 7.7 to 14 kbar is able to stabilize the B19′ phase relative to BCO with a monoclinic angle between 99^0 and 97^0. They also predicted that based on the fact that the lower angle martensite have smaller unit cell volumes relative to BCO, a hydrostatic pressure can also destabilize BCO with respect to B19′ [3]. They attributed the absence of BCO in experiment to the hindering effect of internal stresses to the BCO phase.

Since then many studies have also implemented the B2→BCO MEP using different methods and reached different conclusions about the absence of BCO in experimental observations. Wang et al. attributed the stabilization of B19′ against both B19″ and BCO to an energy barrier in the transformation minimum energy pathway from B2 to B19″ and BCO [70]. However, their conclusion does not seem to be confirmed by other researchers [3,84-86]. Similar to Huang et al., This conclusion is questionable in that there is no conceivable mechanical energy contribution to the destabilization of BCO to one of the other martensitic phases (i.e., B19′ and B19″) from a uniaxial compressive stress. They also showed that smaller twin unit sizes destabilize BCO against B19′ [87], but the effect of the twinning interfaces vanishes by consideration of the larger supercells.

PART 3

THEORETICAL ANALYSIS

3.1. EXPERIMENTAL METHOD

Materials, Nitinol sheets 25 mm * 100 mm * 1 mm, Nitinol wire 25 mm * 100 mm * 1.5 mm the material has not undergone heat treatment. The tests performed to describe the behavior of the substance are.

3.1.1. Tensile Tests

The tests were performed at room temperature, and the temperature change was measured. That occurred while loading (or unloading) samples. An MTS machine was used from the Libya laboratory (College of Technical Engineering, Brak Shati) of the MOP, which allows for periodic elongations of the sample, to be imposed by trunk movement. Different percentages of deformation were used in the tests. The equipment used is compatible with the MTS machine (Figure 3.1).

Figure 3.1. MTS machine.

This machine allows a periodic motion to be imposed on the upper head. It can control the frequency of rotations, and can take values up to 1 Hz. In the Figure. 3.2 provides an overview diagram of the hardware system components.

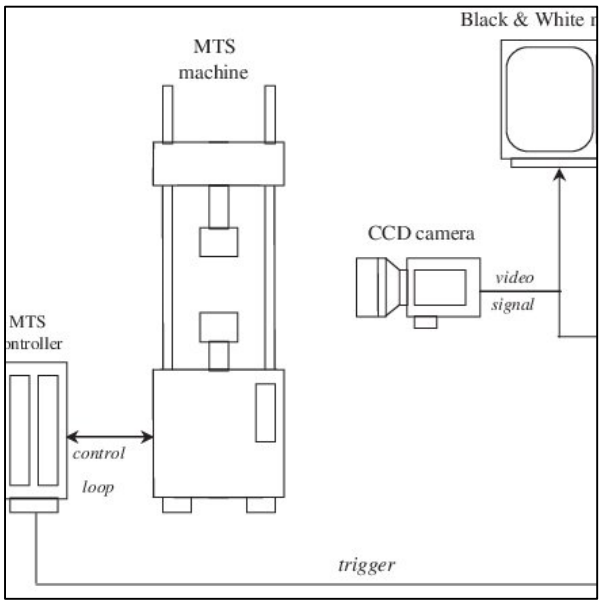

Figure 3.2. MTS machine diagram of the system[88].

The specimens are located between the heads via a system of flat jaws. A Once the specimen is fitted into the jaws, the input data is entered into the computer file, such as the distance between the jaws, the initial stress, the maximum stress, the frequency and the number of cycles. Once the sample was collected, the actual axial stress of the specimen was measured by the MTS 25mm jaw extension gauge. During the sample temperature the test was measured by means of a thermocouple fixed to the center of the test piece.

3.1.2. Leg Movement Control

As a procedure, all tests were performed by assuming the percentage of deformation applied by the device from the gap between the jaws. To determine the distortion ratios imposed on the samples, it was necessary to test with different values, since the actual distortions (measured by the diameter) differ significantly from the distortions imposed by the leg movement.

3.1.3. Temperature Measurement

The temperature of the samples was measured during the tests with a thermocouple which are installed in the center of each sample to be tested. With the digital data collector. Every 0.5 sec the temperature develops at the center of the sample during each test.

The tests were conducted at room temperature, so there may be differences between average temperatures from test to test, for which no type of temperature control tested was performed.

3.1.4. Tests Procedures

The methodology used to develop the experiments is shown below. Mechanical. A schematic diagram is presented (Figure 3.3), to help illustrate some aspects that are indicated in later procedures.

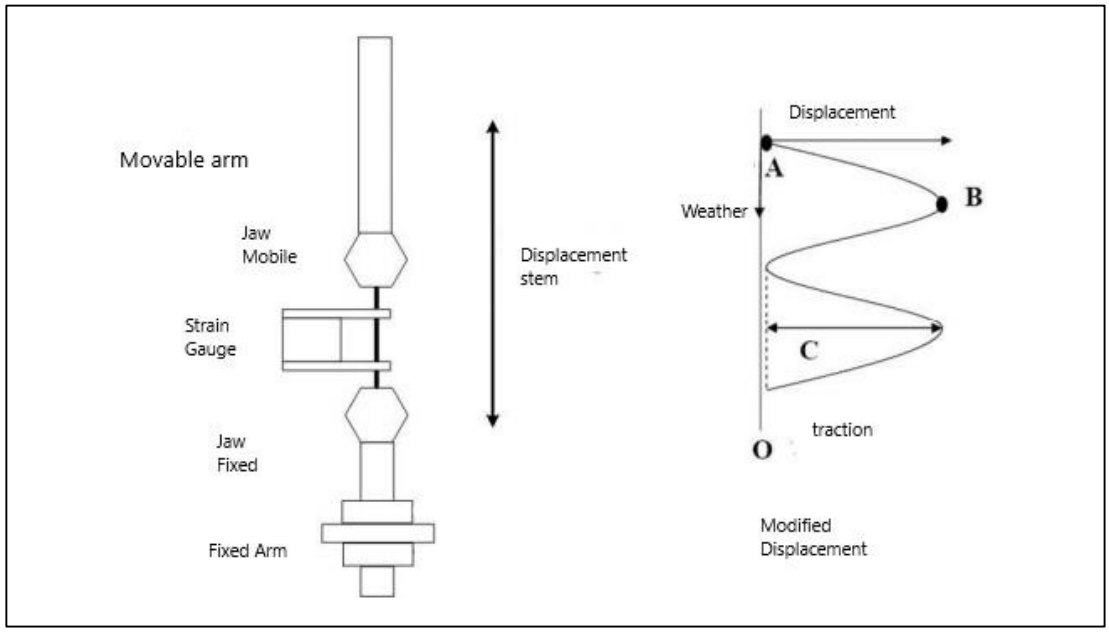

Figure 3.3. Assembly diagram prepared by the researcher.

The system puts the sample in tension until it is broken. The velocity of deformation imposed is the velocity of displacement of the penis. In the case of periodic tests, the

operation of the system consists of a sinusoidal displacement as a result of movement of the upper part of the head. Frequency the sinus displacement is imposed when starting the test, and the upper head's movement velocity is controlled. This offset allows testing of samples at alternating pressure and traction. Tests seek to subject only samples popularity. For this, what was done was to create a deformation by pretending the samples, to prevent them from going into pressure. All mechanical tests performed are controlled by leg displacement.

3.1.4.1. Tensile Test

1.3.4.1.1. Test Program

Samples were drawn to failure to determine stress and maximum deformation. Tests were controlled by deformation, imposing velocity of 0.1 mm / s offset stem.

Total samples: 2.
Samples a and b.

1.3.4.1.2. Take the Test

1. The sample was fitted to the mandible (system's fixed jaw).
2. Then the thermocouple is installed in the center of the sample using elastic bands.
3. Move the (movable) upper jaw, to achieve sufficient clearance in order to be able to locate the dilation scale, but not too large, in order for it to be it has a good grip length on the jaws.
4. Then the sample is fitted into the moving jaw of the system.
5. Install the expansion gauge on the test tube, and make sure the safety is removed and that there is no contact with the jaws.
6. Set the maximum deformation to be done by the machine, as well as adjust the deformation speed.
7. Initiate the data acquisition system and verify the various channels reading is used.

8. Start the test, moving the upper jaw until it reaches break the sample.
9. Broken specimens are removed from the jaws, and both pieces are marked with the same ID.

1.3.4.1.3. Get the Record

In tensile tests to failure, the tension applied to the sample is obtained:

- At every point in time, distortions are measured by diameter and distortions
- It is produced by the movement of the trunk.
- The records obtained have been modified and drawn. Adjustments made.

The following was introduced:

- The values corresponding to the distortion should be taken as a percentage, because the register gives the displacement of the dilation scale in mm, so the values must be divided by the lengths of the starting each of which has the real and nominal distortions.
- The value corresponding to the applied load should be brought into the voltage, divided by the primary region of the sample.
- Due to an initial claim of 0.5% nominal distortion, recording does not start from the original. The initial register offers a load and tension value other than zero. To perform the analysis and graphics the initial distortion was brought to the original, with all results corrected. Using the values of stress and strain, the modulus of elasticity is obtained austenitic or Young's modulus (E), which corresponds to the slope of the initial section of Log (Figure 3.4).

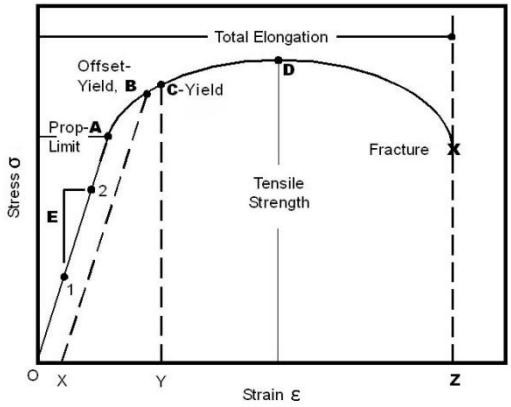

Figure 3.4. Stress deformation curve[89].

The point at which the lines intersect is determined by the shift stress as Figure 3.5.

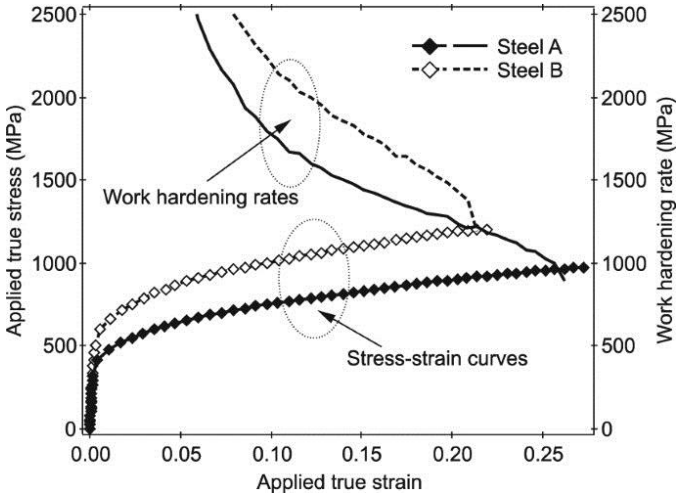

Figure 3.5. Transformation effort [90].

1.3.4.1.4. Samples 1 and 2

At room temperature, two samples were pre-stressed at 0.5% at A. 5% deformation. Cycle at 0.1 Hz. Number of sessions: 10. At room temperature, the same strained samples were pre-tested up to 0.5% at ambient temperature. 7.5% deformation.

Cycle at 0.1 Hz. Number of sessions: 10.
Sample Record 1: CE02A (5%) and CE02B (7.5%).
The temperature record is 1842.

Test tube recording 2: CE02C (5%) and CE02D (7.5%).
The temperature record is 2,175. Deformation control

1.3.4.1.5. Steps to Take the Test

1. Measure the actual dimensions of each sample.
2. Fixation of the sample in the lower jaw (fixed jaw system).
3. Fixation of the thermocouple in the center of the sample using elastic bands.
4. Moving the upper (movable) jaw, to achieve sufficient clearance to be able to locate the dipstick, but not too large, in order to have a good grip length on the jaws.
5. Fitting the sample into the moving jaw of the system.
6. Install the expansion gauge on the specimen, ensuring that the safety is removed and that there is no contact with the jaws.
7. Enter the required parameters for the test. It must be delivered to the instrument of the initial distances between the jaws and between the jaws of the diameter, in addition to the useful section of the sample, the imposition of the initial deformation, the maximum deformation, the number of turns and the frequency.
8. Initiate the data acquisition system and verify the different channels are using reading.
9. Starting the test, moving the upper jaw until it finishes the imposed rotations. When changing the capacity of the tests, one modification is only in the data that is entered into the computer, but the sample remains in the position in which the previous session ended.
10. At the end of the test, stop the machine and continue removing the sample and measuring its dimensions again.

This methodology is controlled by imposed deformation and the specimen should always be pulled. Moreover, since the claim imposed is very low, there is no complication in staying within the range you want to study.

1.3.4.1.6. Get the Record

As a result of the tests, records of displacement of the jaws, and displacement stress gauge and load applied, which must be adjusted. The modifications they have undergone are as follows:

- The values corresponding to the distortions should be taken as a percentage. For this, it should only be multiplied by 100, because the scoring delivers the densimeter and stem offset file as [L / Lo].
- The tension is given as [Kg / cm2, so a transformation of units is performed to bring it to [MPa].
- Through the use of Matlab it was possible to determine the areas under load and Discharging (Figure 3.6). This calculation was performed independently for each cycle of recording.
- Using these two regions, it is possible to determine the inner region of a cycle, which is defined as the subtraction of the two mentioned regions.

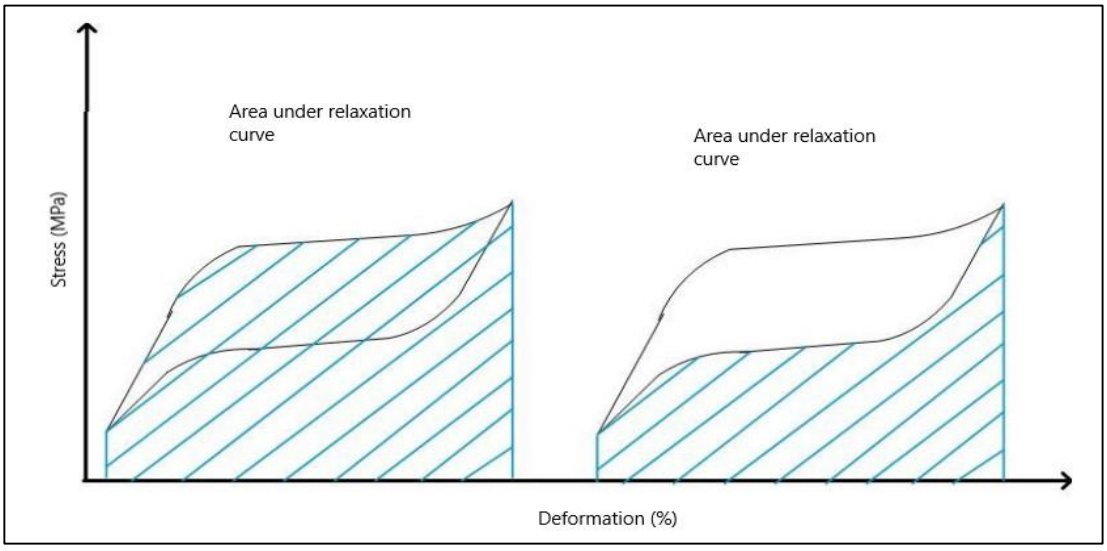

Figure 3.6. Areas calculated by integration.

The hysteresis cycles have different sections, which are representative of the rehearsed phenomena. Therefore, different parameter values were obtained (Figure 3.7) representative of each cycle.

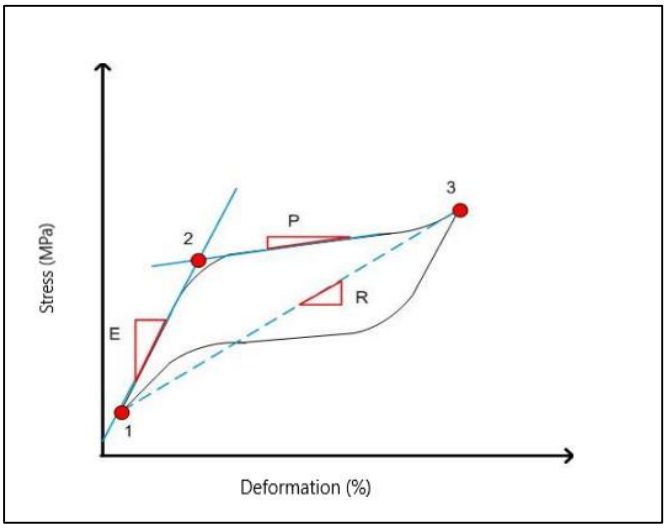

Figure 3.7. Representative parameter values.

Where the parameters to be studied are:

- e: the modulus of austenitic elasticity. The slope of the first section corresponds to a linear curve in tension.
- R: Cycle cutting stiffness. Corresponds to the slope of the auxiliary line drawn from the lowest stress / strain value to the maximum stress strain value.
- P: the slope of the plateau. Corresponds to the slope of the second linear section of the curve.

In a sour state, austenite transforms into a stress-induced martensite:

- 1: The starting point of the test, the lowest stress / strain value.
- 2: Transformation efforts. This value corresponds to the intersection of two lines Auxiliary, where the first is the lengthening of the elastic austenitic section, and the second is an extension of the second linear section (plateau), in which the austenite / martensite transformation is present.

PART 4

EXPERIMENTAL INVESTIGATIONS

4.1. NITINOL MATERIAL

4.1.1. Mechanical Properties of Nitinol

Nitinol or Nickel Titanium (also known as NiTi) is in the unique class of shape memory alloys. Nitinol shape memory alloys can be modified to a great extent by changes in composition, mechanical working and heat treatment [90].

Table 4.1. Transformation properties [90].

Transformation temperature		-200 to 110 deg. C
Latent heat of transformation		5.78 cal/g
Transformation strain (for polycrystalline material)	for a single cycle	max 8%
	for 100 cycles	6%
	for 100,000 cycles	4%
Hysteresis		30 to 50 deg. C

Table 4.2. Nitinol physical properties [90].

Melting point		1300 deg. C (2370 deg. F)
Density		6.45 g/cu.cm (0.233 lb/cu.in)
Thermal conductivity	austenite	0.18 W/cm * deg. C (10.4 BTU/ft * hr * deg. F)
	martensite	0.086 W/cm * deg. C (5.0 BTU/ft * hr * deg. F)
Coefficient of thermal expansion	austenite	11.0E-6/deg. C (6.11E-6/deg. F)
	martensite	6.6E-6/deg. C (3.67E-6/deg. F)
Specific heat		0.20 cal/g * deg. C (0.20 BTU/lb * deg. F)
Corrosion performance		excellent

Table 4.3. Electrical and magnetic properties [90].

Resistivity [resistance = resistivity * length / cross-sectional area]	austenite	approx. 100 micro-ohms * cm (39 micro-ohms * in)
	martensite	approx. 80 micro-ohms * cm (32 micro-ohms * in)
Magnetic permeability		< 1.002
Magnetic susceptibility		3.0E6 emu/g

Table 4.4. Nitinol mechanical properties [90].

Young's modulus****	austenite	approx. 83 GPa (12E6 psi)
	martensite	approx. 28 to 41 GPa (4E6 to 6E6 psi)
Yield strength	austenite	195 to 690 MPa (28 to 100 ksi)
	martensite	70 to 140 MPa (10 to 20 ksi)
Ultimate tensile strength	fully annealed	895 MPa (130 ksi)
	work hardened	1900 MPa (275 ksi)
	Poisson's ratio	0.33
Elongation at failure	fully annealed	25 to 50%
	work hardened	5 to 10%
Hot workability		quite good
Cold workability		difficult due to rapid work hardening
Machinability		difficult, abrasive techniques preferred

4.1.2. Material Composition

This metal alloy is composed of nickel and titanium. It contains these two elements at approximately equal atomic percentages. Nickel is a known allergen, and it might also have carcinogen properties. Due to this reason the nickel content of this alloy has raised great concerns about its usefulness in the medical industry. This metal alloy is composed of nickel and titanium. It contains these two elements at approximately equal atomic percentages. Nickel is a known allergen, and it might also have carcinogen properties. Due to this reason the nickel content of this alloy has raised great concerns about its usefulness in the medical industry.

4.1.3. Corrosion Behavior

4.1.3.1. How Corrosion Resistant Is Nitinol

The corrosion resistance of NiTi alloys is highly dependent on the surface condition. Materials with as-drawn and heat-treated surfaces are more susceptible to pitting corrosion due to the presence of heavy oxide and processing contamination.

Materials with a passive oxide layer, such as mechanically polished or electro polished and then passivated parts, are highly corrosion resistant and have the ability to passivate in the event of a small local destruction of the passive film [92].

4.1.3.2. How do Dissimilar Materials Affect the Corrosion Resistance and Biocompatibility of Niti?

It is highly dependent on the coupling material. Materials such as stainless steels, Ti, and Ta have weak galvanic effects with NiTi and are safer to use as compared to precious metals such as Au and Pt that have strong galvanic effects [92].

4.1.3.3. Is Niti Biocompatible and Can it Be Used as an Implant Material?

NiTi is generally a safe implant material as the FDA has approved many devices for long-term implant applications [92]. According to an in-vitro study of passivated NiTi in Hank's solution, the Ni release rate was the highest of 14.5 x 10-7 mg/cm-2sec-1 in the first day but decreased quickly to an undetectable level in 10 days. In-vivo studies of NiTi implants in soft tissues indicated that the overall inflammatory response to NiTi was very similar to that of stainless steels and Ti-6V-4Al alloy. Studies on NiTi vascular stents showed a mild inflammatory response, minor atrophy of vessel media, acceptable fibro cellular tissue growth and endotheliazation, indicating that the biocompatibility of NiTi stents is equal to or better than that of stainless steel stents. A comparative in-vivo study of NiTi and stainless steel intramedullary rods on osteotomy healing indicated more healed bone unions and closer bone contact for NiTi when compared to the stainless steel group. The callus size and the mineral density were similar between the two groups. Studies on the use of NiTi bone implants in humans generally reported good clinical results. The existing data suggest that NiTi with proper surface finish is a safe biomaterial for vascular, soft tissue and orthopaedic applications [92].

4.2. MECHANICAL TESTS

4.2.1. Tensile To Break Test

Two samples were tested at room temperature, which were drawn with A. The leg movement speed is 0.1 mm / s.

Table 4.5. Details of samples with a diameter of 25 mm tested under tension.

Test sample	Li [mm]	Distance Between Jaws	Temperature Register	File name	
A	70	34.5	1	CE01A	MOP
B	70.11	35.1	140	CB01A	MOP

The trial methodology considered stopping the trial when a certain degree of true deformation, as a safety measure, is because the diameter, which is very sensitive. Also, distortions that exceed 10% of the opening between the jaws of the dilation scale. For this reason, one of the four experiments did not arrive. Fracture before the imposed safety deformation, because this deformation is less than the fracture. Another experiment failed, but the data collection system did not. It worked, so the trial records were not obtained. In one failed experiment, the specimen was deflected, when it reached the safety deformation, it began to compress. Below is a view of the traction curves obtained for the tests performed in Figure 4.1.

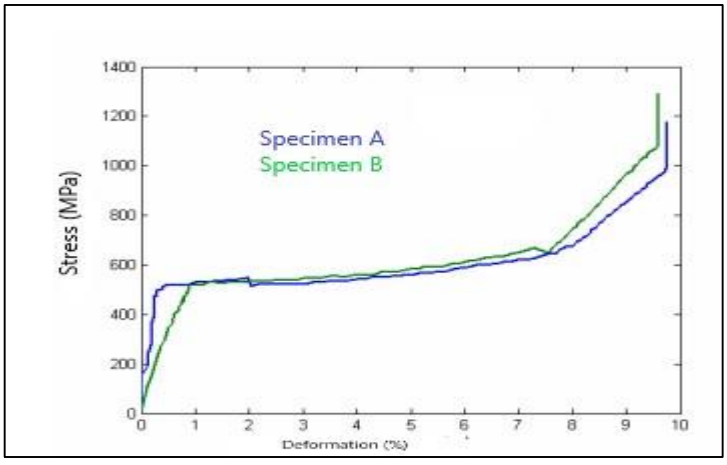

Figure 4.1. The stress versus deformation for monotone fracture tests.

It can be seen that at the beginning of the sample A test, the distortion is not measured. What happened was that the safety of the dipstick wasn't removed at the start of the test, but A. Soon after, causing the first true abnormalities not to be recorded. If from the sample B test, the pressure decreased by about 8% from distortion. The exact cause of the voltage loss cannot be determined, however this could be because the specimen may have slipped slightly from either jaw.

4.2.2. Temperature Change

As the load is applied to the samples, there is great variability in the temperature. The temperature variation over time has been plotted below (Figure 4.2).

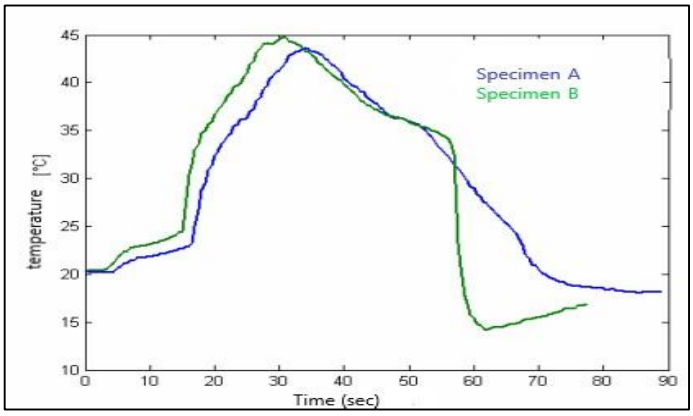

Figure 4.2. Stress vs. deformation and temperature vs. distortion..

It can be seen that the temperature of the test piece B shows a sudden drop is not. It is observed in sample A by analyzing both graphs together (Figure 4.2), it can be seen that the temperature increases with a deformation of the austenitic phase. After crawling the temperature continues to rise, reaching a maximum of about 4% distortion.

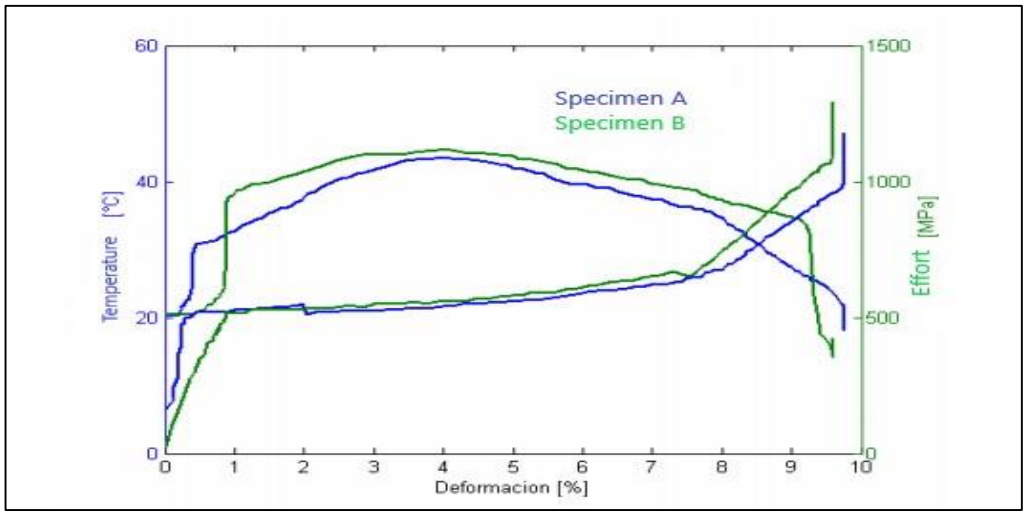

Figure 4.3. Stress vs. deformation and temperature vs. distortion.

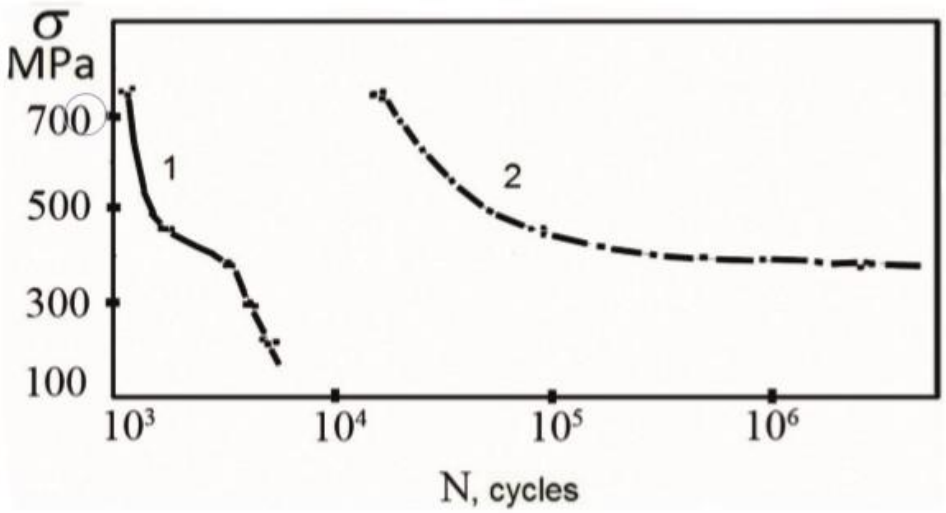

Figure 4.4. Fatigue curves of a nanostructural nitinol before treatment (1) and after annealing at 450°C, 15 min (2).

4.2.3. Representative Numerical Values

In both cases, the rupture was obtained in the area near the jaws, (A) until fraction. (B) Compression when the machine is rolled back. Table 4.2 shows the characteristic values of a tensile test, such as austenitic elastic modulus, transformation stress, maximum stress and percentage maximum deformation.

Table 4.6. Representative values of tensile tests.

Property	Specimen A	Specimen B
Deformation by pretension	0.5%	0,5%
Modulus of Elasticity (GPa)	---	51,4
Transformation Stress (MPa)	495,7	519.11
Maximum Tension (MPa)	1176,2	1298,42
Maximum deformation (%)	9,6	9,6

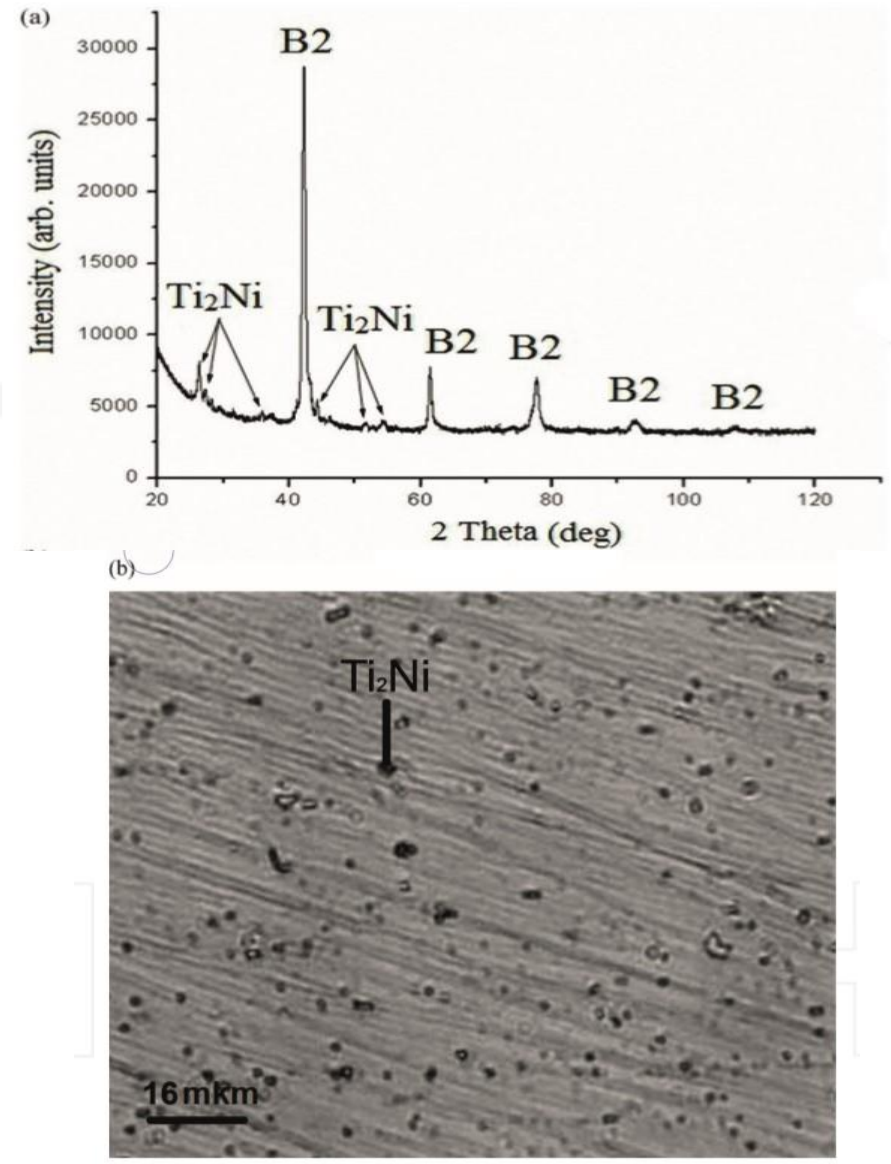

Figure 4.5. Nitinol structure data: (a) X-ray diffraction patterns and (b) Microstructure analysis.

Bright and dark spot combinations differ A high content of titanium oxide is detected in bright colors and carbon, in dark places. Both layers are 3 μm thick and are not placed on top of each other. This thickened surface layer was, as it was believed, the result of a long heat intermediate treatment during wire production.

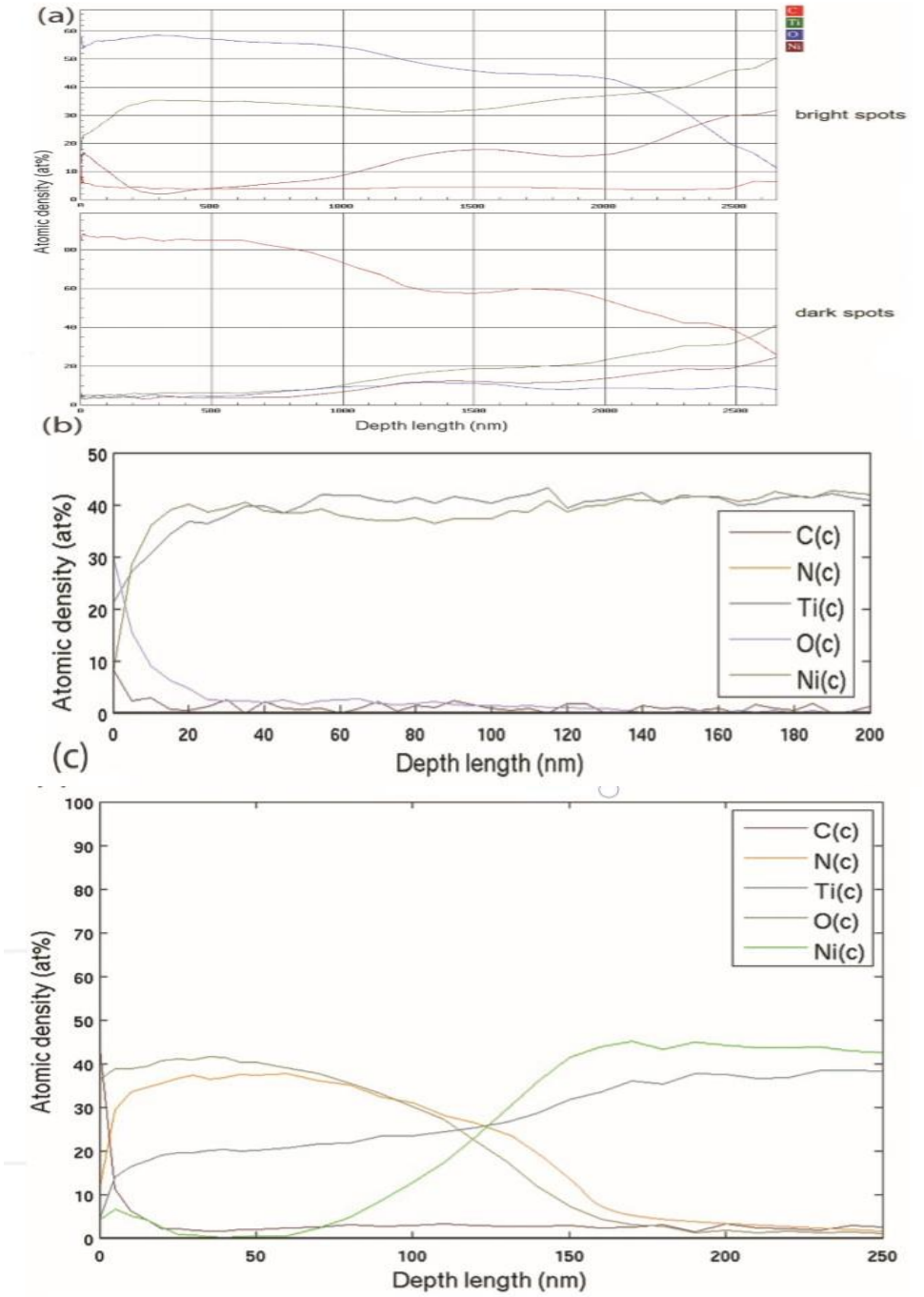

Figure 4.6. Wire configuration for Auger surface wire before immersion: (a) Prior to treatment; after rinsing; (b) After polishing; and (c) Polishing and rinsing (dark and light spots in Figures 3a and b).

4.3. DISCUSSION OF THE TESTS

Thesis titled Operation Training and its Effects on Operating Stress for Nitinol-Form Memory Wires by Pete A. ROCO Introduction to Graduate School as a partial fulfillment of the requirements for a Master of Science in Mechanical Engineering Originally, this test attempted to repeat Test # 4.2, but because the parameters are entered differently and the relationships between actual and imposed distortions differ in each device, it was not possible to obtain a distortion equal to that of Test. Although the distortions obtained are not the same, the results are very helpful to make a comparison with what has actually been accomplished. The results are found in Figures 4.7 and 4.8.

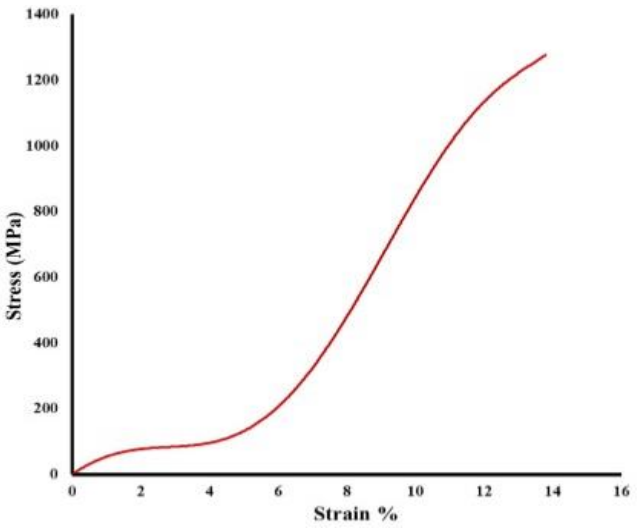

Figure 4.7. Monotonic tensile test findings results.

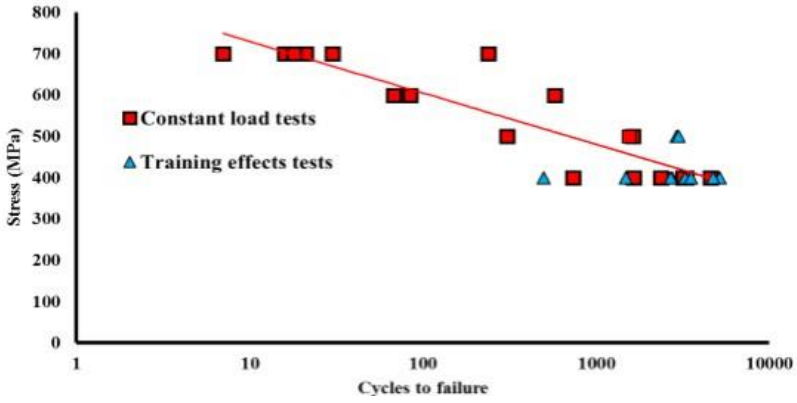

Figure 4.8. Stress versus NNff data with and without training samples.

PART 5

CONCLUSION AND RECOMMENDATIONS

5.1. CONCLUSION

Nickel titanium, also known as nitinol, is an alloy metal of nickel and titanium, in which the two elements are present in roughly equal atomic proportions. The different alloys are named according to the weight ratio of nickel, for example Nitinol 55 and Nitinol 60. The shape memory exhibits superior impact and flexibility at different temperatures.

Nitinol alloys display two unique properties that are closely related: shape-memory effect and superior elasticity (also called pseudo-elasticity). Shape memory is the ability of nitinol to undergo deformation at one temperature, maintain its deformed shape when external force is removed, then restore its original undistorted shape upon heating above the “transition temperature.” Ultimate elasticity is the ability of a mineral to undergo significant deformations and immediately return to its shape. Not deformed when removing the external load. Nitinol can tarnish 10-30 times more than regular metals and return to its original form. Whether the nitinol behaves with the shape memory effect or the super elasticity depends on whether it is above the transition temperature of the specific alloy. Under the transition temperature the shape memory effect appears, and above this temperature it behaves miraculously. Nitinol's unusual properties are derived from a reversible solid-state phase shift known as a martensitic transformation, between two different phases of martensite crystals, requiring 10,000-20,000 pounds per square inch (69-138 MPa) of mechanical stress.

At higher temperatures, nitinol assumes a simple, overlapping cubic structure referred to as austenite (also known as the parent phase). At lower temperatures,

nitinol spontaneously transforms into a more complex monocrystalline structure known as martensite (daughter stage). There are four transition temperatures associated with the transformations of austenite to martensite and martensite to austenite. Starting with complete austenite, martensite begins to form when the alloy is cooled to what is called the start of martensite temperature, or MS, and the temperature at which the conversion is complete is called martensite finish temperature, or F. When the alloy is fully martensitic and undergoes heating, austenite begins to form at the beginning of the austenite temperature, AC, and ends at the temperature of the austenite finish.

The cooling / heating cycle shows the hysterectomy. The width of hysteresis depends on the exact composition and processing of the nitinol; its typical value is a temperature range that extends around 20-50 K (20-50 ° C; 36-90 ° F) but can be reduced or amplified by alloying and processing. A critical factor in the properties of nitinol are two major aspects of this phase shift. The first is that the transformation is "reversible," which means that heating above the transition temperature will return the crystal structure to the simpler austenite phase. The second key point is that the reversal in both directions is immediate.

The crystal structure of martensite (known as monoclinic or B19 structure) has the unique ability to undergo limited deformation in some ways without breaking atomic bonds. This type of deformation is known as twinning, which consists of rearranging the atomic planes without causing slipping or permanent deformation. It is able to undergo approximately 6-8% stress in this way. When martensite is returned to austenite by heating, the original austenitic structure is restored, regardless of whether the martensite phase is deformed or not. Thus the name “shape memory” refers to the fact that the shape of the austenite phase at a high temperature is “remembered”, even though the alloy is strongly deformed at a lower temperature. A great deal of pressure can be induced by preventing the reflux of deformed martensite into austenite - from 35,000 psi to more than 100,000 psi (689 MPa) in many cases. One of the reasons why nitinol works so hard to return to its original form is that it is not just an ordinary metal alloy, but what is known as an inter-mineral compound. In an ordinary alloy, the components are randomly placed in the

crystal lattice; In an ordered metal compound, the atoms (in this case, nickel and titanium) have very specific sites in the lattice. The fact that nitinol is a mineral is largely responsible for the complexity of manufacturing devices made of alloys.

The scenario described above (cooling of austenite to form a martensite, distorting the martensite, then heating to return to austenite, thus returning the original undistorted form) is known as the thermoregulation memory effect. To fix the original "original shape" the alloy must be held in place and heated to about 500 ° C (932 ° F). Usually this process is called shaping. A second effect called superelasticity or pseudoelasticity has also been observed in nitinol. This effect is a direct result of the fact that martensite can be formed by pressure as well as by cooling. Thus in a certain temperature range one can compress austenite, causing a martensite to form while simultaneously changing shape. In this case, once the pressure is removed, the nitinol will automatically return to its original form. In this method of use, Nitinol behaves like a super-spring, which possesses an elastic range 10 to 30 times greater than that of regular spring material. However, there are limitations: the effect is only observed around 273-313 K (0-40 ° C; 32-104 ° F) above the AF temperature. This upper limit is referred to as M d, which corresponds to the highest temperature that can still cause stress forming a martensite. Less than Md, the martensite formation under load allows for superior flexibility due to its twinning. Because martensite is no longer forming, the only response to stress is a slip of the austenitic microstructure, and thus permanent deformation.

Nitinol typically consists of about 50 to 51% atomic percent nickel (55 to 56% weight percent). Small changes in composition can dramatically change the alloy transition temperature. The nitinol transition temperatures are somewhat controllable, with AF temperature ranging from around -20 ° C to +110 ° C. Thus, it is common to refer to the nitinol formulation as "super flexible" or "austenitic" if A F is lower than the reference temperature, while "shape memory" or "martensite" if it is higher. Reference temperature is usually defined as room temperature or human body temperature (37 ° C, 98 ° F).

One of the effects that often occurs with respect to nitinol is the so-called R-phase. The R stage is another martensite stage that competes with the martensite stage. Since it does not present the significant memory effects of the martensitic phase, it is usually impractical.

The ability of nickel-titanium alloys to recover their initial state after expansion depends on the material's deformation and temperature. If a material undergoes deformation at low temperatures, it can return to its original shape by increasing its temperature above a certain level called Af (end of the austenitic phase), and if it deforms at high temperatures, the material instantly takes shape. In the second case, it is called a super-elastic material.

Generally, this shape is preserved after machining at a high temperature. This temperature is called the memory temperature. If it is then denatured at the application temperature, usually at room temperature or a certain low temperature, it reverts to the previously preserved shape.

Shape memory alloys are relatively new to medical applications, so there is little experience with using these materials. In this study, the mechanical behavior of a 1.5 mm diameter nitinol wire was examined experimentally.

After the mechanical behavior of Nitinol rods has been distinguished and subjected to tensile tests at room temperature and at different frequencies, the superelastic behavior of the material can be evaluated. From tensile to rupture tests, it can be concluded that the material is deformed at approximately 10% of its initial useful length before it reaches the fracture, and that the failure stress is about 1,300 MPa. When the fault is reached, the material does not present areas in which its cross section is reduced, so the location of the fault cannot be predicted. In this case the failures occurred near the jaws, which could happen because the machine was not designed to test the rods, and also because the sample size is too small, making assembly difficult without creating unwanted stresses in the tape. This is it indicates that the refractive stress is not pure stress and therefore the limit present is lower with respect to the pure stress.

With regard to tensile tests, it may be noted that the representative numerical values fall within the ranges indicated in other studies referred to in this standard. When the results presented in this study are finally evaluated, it can be considered that the general and specific goals raised have been achieved. Nitinol's ability to dissipate energy has been studied through periodic tests, and it has been verified that the material is super flexible, confirming the results presented by different authors. By obtaining results similar to those in the literature

5.2. RECOMMENDATIONS

As it became apparent, despite the fact that nitinol (TiNi) is a commercial (and non-commercial) shape memory alloy, it is necessary, for the sake of completeness, to mention some other alloys that are able to exhibit completely similar properties to the main class of the classes in question, albeit To a much lesser degree.

As for the considerations reported regarding the biocompatibility properties of nitinol, which, as indicated, are adversely affected by the presence of nickel, an additional form memory material called nickel-free has been studied and developed, along with titanium, the main component of the alloy. : Among all that is possible Definitely remember Ti-Nb-Al, which can reach 6% elastic deformation values, Ti-Nb-Ta-Zr, Ti-Nb-Sn and Ti-Mo-Ga.

While keeping the chemical composition of the alloy unchanged, one of the most common and well-known variants of common nitinol, the substance mainly treated here, is so-called porous nitinol. In certain circumstances, it represents the absolutely preferred material, on the one hand for the properties of shape memory, with which this substance persists even in the porous formation, and on the other hand for what distinguishes it from the common nitinol. The porosity of the material, in fact, and thus also the porosity of the shape memory alloy, particularly for applications in the orthopedic field, is a factor, albeit not critical, definitely noteworthy in terms of bone regeneration and thus biocompatibility, on the one hand to obtain a greater contact surface with tissues Bones, on the other hand, because of the possibility of circulating body fluids within the pores of the organ itself

In conclusion, to date memory materials, in particular nitinol, represent, in certain circumstances, an important and, in those cases, the best alternative to traditional metal alloys for applications in the biomedical field. On the one hand, they undoubtedly have unique shape-memory properties, and on the other hand, their remarkable mechanical properties and biocompatibility. For these reasons, they are still the subject of much research in the biomedical and industrial fields.

.

REFERENCES

1. Lane, R., and Craig, B., "Materials that sense and respond- An introduction to smart materials", ***AMPTIAC Newsletter,*** *7*(2): 9-14 (2003).

2. Newnham, R. E., "Piezoelectric sensors and actuators: smart materials", **In** ***Proceedings of the 1992 IEEE Frequency Control Symposium,*** 4(9):513-524 (1992).

3. Otsuka, K., and Wayman, C. M., "Shape memory materials", ***Cambridge University Press,*** London, UK, 23-33 (1999).

4. Anantachaisilp, F., "Fabrication of shape memory alloys using affordable additive manufacturing routes", ***Naval Postgraduate School Monterey United States,*** USA, 34-44 (2018).

5. Spillman Jr, W. B., Sirkis, J. S., and Gardiner, P. T., "Smart materials and structures: what are they?", ***Smart Materials and Structures,*** 5(3): 247 (1996).

6. Hongsheng, H., Juan, W., Liang, C., Jiong, W., and Xuezheng, J., "Design, control and test of a magnetorheological fluid fan clutch", ***In 2009 IEEE International Conference on Automation and Logistics,*** Shenyang, China, 1248-1253 (2009).

7. Miyazaki, S., Otsuka, K., and Wayman, C. M., "The shape memory mechanism associated with the martensitic transformation in Ti Ni alloys—I. Self-accommodation", ***Acta Metallurgica,*** 37(7): 1873-1884 (1989).

8. Guo, S., Dong, X., Wang, G., Lu, F., Kang, H., and Wang, Y., "Properties evaluation of piezoelectric materials in application of cochlear implant", ***Ferroelectrics,*** 413(1): 272-278 (2011).

9. Konak, M. J., Powlesland, I. G., van der Velden, S. P., and Galea, S. C., "Analysis of a self-powered piezoelectric vibration damper", ***In Smart Structures and Devices International Society for Optics and Photonics,*** 42(35): 328-339 (2001).

10. Kuribayashi, K., "Micro SMA actuator and motion control", **In** ***MHS2000. Proceedings of 2000 International Symposium on Micro mechatronics and Human Science (Cat. No. 00TH8530),*** Nagoya, Japan, 35-42 (2000).

11. Fu, Z., Yuan, M., Sun, D., and Liu, W., "Research of piezoelectric sensor array in structural health monitoring", ***In Seventh International Symposium on Instrumentation and Control Technology: Sensors and Instruments, Computer Simulation, and Artificial Intelligence International Society for Optics and Photonics,*** 7(12):717 (2008).

12. Rocha, J. G., Goncalves, L. M., Rocha, P. F., Silva, M. P., and Lanceros-Mendez, S., "Energy harvesting from piezoelectric materials fully integrated in footwear", ***IEEE Transactions on Industrial Electronics,*** 57(3): 813-819 (2009).

13. Lynch, B. K., "Modeling fo the stress-strain-resistance behaviour of Ni-Ti and Ni-Ti-Cu shape memory alloys for use in sensor less actuator position control", ***Doctoral Dissertation, Carleton University***, Ottawa, Canada, 34-51 (2013).

14. Aboudi, J., "The response of shape memory alloy composites", ***Smart Materials and Structures,*** 6(1): 1 (1997).

15. Ray, M. C., and Pradhan, A. K., "On the use of vertically reinforced 1-3 piezoelectric composites for hybrid damping of laminated composite plates", ***Mechanics of Advanced Materials and Structures,*** 14(4): 245-261 (2007).

16. Straub, F. K., and Merkley, D. J., "Design of a smart material actuator for rotor control", ***In Smart Structures and Materials 1995: Smart Structures and Integrated Systems,*** 24(43): 89-104 (1995).

17. Mavroidis, C., Pfeiffer, C., and Mosley, M., "5.1 conventional actuators, shape memory alloys, and electrorheological fluids", ***Automation, miniature robotics, and sensors for nondestructive testing and evaluation***, 4(3): 189 (2000).

18. Otsuka, K., and Ren, X., "Recent developments in the research of shape memory alloys", ***Intermetallics,*** *7*(5): 511-528 (1999).

19. Mavroidis, C., "Development of advanced actuators using shape memory alloys and electrorheological fluids", ***Journal of Research in Nondestructive Evaluation,*** 14(1): 1-32 (2002).

20. Rahman, M. A., "Patents on superplastic shape memory alloy", ***Recent Patents on Mechanical Engineering,*** 1(1): 65-67 (2008).

21. Gil, F. J., and Planell, J. A., "Shape memory alloys for medical applications", ***Proceedings of the Institution of Mechanical Engineers, Part H: Journal of Engineering in Medicine,*** 212(6): 473-488 (1998).

22. Buehler, W. J., Gilfrich, J. V., and Wiley, R. C., "Effect of low- temperature phase changes on the mechanical properties of alloys near composition TiNi", ***Journal of Applied Physics,*** 34(5): 1475-1477 (1963).

23. Okamoto, H., and Okamoto, H., "Phase diagrams for binary alloys", ***Materials Park, OH: ASM international,*** USA, 67-71 (2000).

24. Okamoto, H., and Massalski, T. B., "Binary alloy phase diagrams requiring further studies", ***Journal of Phase Equilibria***, 15(5): 500-521 (1994).

25. Nishida, M., Wayman, C. M., and Honma, T., "Precipitation processes in near-equiatomic TiNi shape memory alloys", ***Metallurgical Transactions A,*** 17(9): 1505-1515 (1986).

26. Otsuka, K., and Ren, X., "Physical metallurgy of Ti–Ni-based shape memory alloys", ***Progress in Materials Science,*** 50(5): 511-678 (2005).

27. Liu, Y., Blanc, M., Tan, G., Kim, J. I., and Miyazaki, S., "Effect of ageing on the transformation behaviour of Ti–49.5 at% Ni", ***Materials Science and Engineering: A,*** 43(8): 617-621 (2006).

28. Tirry, W., and Schryvers, D., "Quantitative determination of strain fields around Ni4Ti3 precipitates in NiTi", ***Acta Materialia***, 53(4): 1041-1049 (2005).

29. Yang, Z., Tirry, W., and Schryvers, D., "Analytical TEM investigations on concentration gradients surrounding Ni4Ti3 precipitates in Ni–Ti shape memory material", ***Scripta Materialia,*** 52(11): 1129-1134 (2005).

30. Allafi, J. K., Ren, X., and Eggeler, G., "The mechanism of multistage martensitic transformations in aged Ni-rich NiTi shape memory alloys", ***Acta Materialia,*** 50(4): 793-803 (2002).

31. Zou, W. H., Han, X. D., Wang, R., Zhang, Z., Zhang, W. Z., and Lai, J. K. L., "TEM and HREM study of the interphase interface structure of Ti3Ni4 precipitates and parent phase in an aged TiNi shape memory alloy", ***Materials Science and Engineering: A,*** 219(2): 142-147 (1996).

32. Wang, X. B., Verlinden, B., and Van Humbeeck, J., "R-phase transformation in NiTi alloys", ***Materials Science and Technology,*** 30(13): 1517-1529 (2014).

33. Kibey, S., Sehitoglu, H., and Johnson, D. D., "Energy landscape for martensitic phase transformation in shape memory NiTi", ***Acta Materialia,*** 57(5): 1624-1629 (2009).

34. Kajiwara, S., "Strengthening of Ti-Ni shape-memory films by coherent subnanometric plate precipitates", ***Philosophical Magazine Letters,*** 74(3): 137-144 (1996).

35. Nishida, M., and Honma, T., "All-round shape memory effect in Ni-rich TiNi alloys generated by constrained aging", ***Scripta Metallurgica,*** 18(11): 1293-1298 (1984).

36. Schryvers, D., and Potapov, P. L., "R-phase structure refinement using electron diffraction data", ***Materials Transactions,*** 43(5): 774-779 (2002).

37. Ishida, S., and Asano, S., "R-phase and Electronic Structures of TiNi and TiNi8/9Fe1/9", ***Materials Transactions,*** 43(5): 780-784 (2002).

38. Tang, W., "Thermodynamic study of the low-temperature phase B19′ and the martensitic transformation in near-equiatomic Ti-Ni shape memory alloys", ***Metallurgical and Materials Transactions A,*** 28(3): 537-544 (1997).

39. Hatcher, N., Kontsevoi, O. Y., and Freeman, A. J., "Role of elastic and shear stabilities in the martensitic transformation path of NiTi", ***Physical Review B,*** 80(14): 144203 (2009).

40. Mahmud, A. S., Wu, Z., Yang, H., and Liu, Y., "Effect of cold work and partial annealing on thermomechanical behaviour of Ti-50.5 at% Ni", ***Shape Memory and Superelasticity,*** 3(1): 57-66 (2017).

41. Uchil, J., Kumara, K. G., and Mahesh, K. K., "Effect of thermal cycling on R-phase stability in a NiTi shape memory alloy", ***Materials Science and Engineering: A,*** 332(2): 25-28 (2002).

42. Lagoudas, D. C., "Shape memory alloys: modeling and engineering applications", ***Springer Science and Business Media,*** Berlin, Germany, 23-33 (2008).

43. Tang, W., Sandström, R., Wei, Z. G. and Miyazaki, S., "Experimental investigation and thermodynamic calculation of the Ti-Ni-Cu shape memory alloys", ***Metallurgical and Materials Transactions A,*** 31(10): 2423-2430 (2000).

44. Gou, L., Liu, Y., and Ng, T. Y., "An investigation on the crystal structures of Ti50Ni50− xCux shape memory alloys based on density functional theory calculations", ***Intermetallics,*** 5(3): 20-25 (2014).

45. Liu, Y., and McCormick, P. G., "Thermodynamic analysis of the martensitic transformation in NiTi—I. Effect of heat treatment on transformation behaviour", ***Acta Metallurgica ET Materialia,*** 42(7): 2401-2406 (1994).

46. Nam, T. H., Saburi, T., Nakata, Y., and Shimizu, K. I., "Shape memory characteristics and lattice deformation in Ti–Ni–Cu alloys", ***Materials Transactions,*** 31(12): 1050-1056 (1990).

47. Liu, Y., and Galvin, S. P., "Criteria for pseudoelasticity in near-equiatomic NiTi shape memory alloys", ***Acta Materialia,*** 45(11): 4431-4439 (1997).

48. Nam, T. H., Saburi, T., and Shimizu, K. I., "Cu-content dependence of shape memory characteristics in Ti–Ni–Cu alloys", ***Materials Transactions,*** 31(11): 959-967 (1990).

49. Huang, X., Ackland, G. J., and Rabe, K. M., "Crystal structures and shape-memory behaviour of NiTi", ***Nature Materials,*** 2(5): 307-311 (2003).

50. Vishnu, K. G., and Strachan, A., "Phase stability and transformations in NiTi from density functional theory calculations", ***Acta Materialia,*** 58(3): 745-752 (2010).

51. Khalil-Allafi, J., Dlouhy, A., and Eggeler, G., "Ni4Ti3-precipitation during aging of NiTi shape memory alloys and its influence on martensitic phase transformations", ***Acta Materialia,*** 50(17): 4255-4274 (2002).

52. Kudoh, Y., Tokonami, M., Miyazaki, S., and Otsuka, K., "Crystal structure of the martensite in Ti-49.2 at.% Ni alloy analyzed by the single crystal X-ray diffraction method", ***Acta Metallurgica***, 33(11): 2049-2056 (1985).

53. Zheng, Y., Jiang, F., Li, L., Yang, H., and Liu, Y., "Effect of ageing treatment on the transformation behaviour of Ti–50.9 at.% Ni alloy", ***Acta Materialia,*** 56(4): 736-745 (2008).

54. Grossmann, C., Frenzel, J., Sampath, V., Depka, T., and Eggeler, G., "Elementary transformation and deformation processes and the cyclic stability of NiTi and NiTiCu shape memory spring actuators", ***Metallurgical and Materials Transactions A,*** 40(11): 2530-2544 (2009).

55. Cui, J., Chu, Y. S., Famodu, O. O., Furuya, Y., Hattrick-Simpers, J., James, R. D. and Takeuchi, I., "Combinatorial search of thermoelastic shape-memory alloys with extremely small hysteresis width", ***Nature Materials,*** 5(4): 286-290 (2006).

56. Lin, H. C., and Wu, S. K., "Determination of heat of transformation in a cold-rolled martensitic TiNi alloy", ***Metallurgical Transactions A,*** 24(2): 293-299 (1993).

57. Sehitoglu, H., Jun, J., Zhang, X., Karaman, I., Chumlyakov, Y., Maier, H. J., and Gall, K., "Shape memory and pseudoelastic behavior of 51.5% Ni–Ti single crystals in solutionized and overaged state", ***Acta Materialia,*** 49(17): 3609-3620 (2001).

58. Fan, G., Chen, W., Yang, S., Zhu, J., Ren, X., and Otsuka, K., "Origin of abnormal multi-stage martensitic transformation behavior in aged Ni-rich Ti–Ni shape memory alloys", ***Acta Materialia,*** 52(14): 4351-4362 (2004).

59. Bakhtiari, R., Shariat, B. S., Motazedian, F., Wu, Z., Zhang, J., Yang, H., and Liu, Y., "Complex transformation field created by geometrical gradient design of NiTi shape memory alloy", ***Functional Materials Letters,*** 10(10): 1740-1780 (2017).

60. Shariat, B. S., Meng, Q., Mahmud, A. S., Wu, Z., Bakhtiari, R., Zhang, J. and Liu, Y., "Functionally graded shape memory alloys: Design, fabrication and experimental evaluation", ***Materials and Design,*** 12(4): 225-237 (2017).

61. Jiang, F., Liu, Y., Yang, H., Li, L., and Zheng, Y., "Effect of ageing treatment on the deformation behaviour of Ti–50.9 at.% Ni", ***Acta Materialia,*** 57(16): 4773-4781 (2009).

62. Liu, Y., Kim, J. I., and Miyazaki, S., "Thermodynamic analysis of ageing-induced multiple-stage transformation behavior of NiTi", ***Philosophical Magazine,*** 84(20): 2083-2102 (2004).

63. Dlouhy, A., Khalil-Allafi, J. and Eggeler, G., "Multiple-step martensitic transformations in Ni-rich NiTi alloys--an in-situ transmission electron microscopy investigation", ***Philosophical Magazine,*** 83(3): 339-363 (2003).

64. Firstov, G. S., Vitchev, R. G., Kumar, H., Blanpain, B., and Van Humbeeck, J., "Surface oxidation of NiTi shape memory alloy", ***Biomaterials,*** 23(24): 4863-4871 (2002).

65. Khalil-Allafi, J., Eggeler, G., Schmahl, W. W., and Sheptyakov, D., "Quantitative phase analysis in microstructures which display multiple step martensitic transformations in Ni-rich NiTi shape memory alloys", ***Materials Science and Engineering: A,*** 43(8): 593-596 (2006).

66. Meng, Q., Yang, H., Liu, Y., and Nam, T. H., "Compositionally graded NiTi plate prepared by diffusion annealing", ***Scripta Materialia,*** 67(3): 305-308 (2012).

67. Li, H. X., Mao, S. C., Zang, K. T., Liu, Y., Guo, Z. X., Wang, S. B. and Yin, X. Q., "An in situ TEM study of the size effect on the thermally induced martensitic transformation in nanoscale NiTi shape memory alloy", ***Journal of Alloys and Compounds,*** 58(8): 337-342 (2014).

68. Fujishima, K., Nishida, M., Morizono, Y., Yamaguchi, K., Ishiuchi, K., and Yamamuro, T., "Effect of heat treatment atmosphere on the multistage martensitic transformation in aged Ni-rich Ti–Ni alloys", ***Materials Science and Engineering: A,*** 43(8): 489-494 (2006).

69. Chu, C. L., Hu, T., Wu, S. L., Dong, Y. S., Yin, L. H., Pu, Y. P. and Chu, P. K., "Surface structure and properties of biomedical NiTi shape memory alloy after Fenton's oxidation", ***Acta Biomaterialia,*** *3*(5): 795-806 (2007).

70. Mahmud, A. S., Liu, Y., and Nam, T. H., "Gradient anneal of functionally graded NiTi", ***Smart Materials and Structures,*** 17(1): 15-31 (2008).

71. Pohl, M., Glogowski, T., Kühn, S., Hessing, C., and Unterumsberger, F., "Formation of titanium oxide coatings on NiTi shape memory alloys by selective oxidation", ***Materials Science and Engineering: A,*** 48(1): 123-126 (2008).

72. Armitage, D. A., Parker, T. L., and Grant, D. M., "Biocompatibility and hemocompatibility of surface- modified NiTi alloys", ***Journal of Biomedical Materials Research Part A: An Official Journal of the Society For Biomaterials, the Japanese Society for Biomaterials, and the Australian Society for Biomaterials and the Korean Society for Biomaterials***, 66(1): 129-137 (2003).

73. Undisz, A., Hanke, R., Freiberg, K. E., Hoffmann, V., and Rettenmayr, M., "The effect of heating rate on the surface chemistry of NiTi", ***Acta Biomaterialia,*** 10(11): 4919-4923 (2014).

74. Chan, C. M., Trigwell, S., and Duerig, T., "Oxidation of a NiTi alloy", ***Surface and Interface Analysis,*** 15(6): 349-354 (1990).

75. Undisz, A., Schrempel, F., Wesch, W., and Rettenmayr, M., "In situ observation of surface oxide layers on medical grade Ni- Ti alloy during straining", ***Journal of Biomedical Materials Research Part A: An Official Journal of the Society for Biomaterials, the Japanese Society for Biomaterials, and the Australian Society for Biomaterials and the Korean Society for Biomaterials,*** 88(4): 1000-1009 (2009).

76. Delaey, L., Krishnan, R. V., Tas, H., and Warlimont, H., "Thermoelasticity, pseudoelasticity and the memory effects associated with martensitic transformations", ***Journal of Materials Science,*** 9(9): 1521-1535 (1974).

77. Miller, D. A., and Lagoudas, D. C., "Influence of cold work and heat treatment on the shape memory effect and plastic strain development of NiTi", ***Materials Science and Engineering: A,*** 308(2): 161-175 (2001).

78. Karaca, H. E., Acar, E., Tobe, H., and Saghaian, S. M., "NiTiHf-based shape memory alloys", ***Materials Science and Technology,*** 30(13): 1530-1544 (2014).

79. Liu, Y., Xie, Z., Van Humbeeck, J., and Delaey, L., "Asymmetry of stress–strain curves under tension and compression for NiTi shape memory alloys", ***Acta Materialia,*** 46(12): 4325-4338 (1998).

80. Miller, D. A., and Lagoudas, D. C., "Thermomechanical characterization of NiTiCu and NiTi SMA actuators: influence of plastic strains", ***Smart Materials and Structures,*** 9(5): 640 (2000).

81. Sittner, P., Liu, Y. and Novák, V., "On the origin of Lüders-like deformation of NiTi shape memory alloys", ***Journal of the Mechanics and Physics of Solids,*** 53(8): 1719-1746 (2005).

82. Shi, X. B., Guo, F. M., Zhang, J. S., Ding, H. L., and Cui, L. S., "Grain size effect on stress hysteresis of nanocrystalline NiTi alloys", ***Journal of Alloys and Compounds,*** 68(8): 62-68 (2016).

83. Xiao, Y., Zeng, P., and Lei, L., "Grain size effect on mechanical performance of nanostructured superelastic NiTi alloy", ***Materials Research Express,*** 4(3): 35-702 (2017).

84. Krulevitch, P., Lee, A. P., Ramsey, P. B., Trevino, J. C., Hamilton, J., and Northrup, M. A., "Thin film shape memory alloy microactuators", ***Journal of Microelectromechanical Systems,*** 5(4): 270-282 (1996).

85. Neshev, I., Vichev, R. G., Tzanev, S., and Todorov, S. S., "Sputtering of NiTi alloys: a comparison of experiment and simulation", ***Vacuum,*** 44(4): 209-212 (1993).

86. Shih, C. L., Lai, B. K., Kahn, H., Phillips, S. M., and Heuer, A. H., "A robust co-sputtering fabrication procedure for TiNi shape memory alloys for MEMS", ***Journal of Microelectromechanical Systems***, 10(1): 69-79 (2001).

87. Shin, D. D., Lee, D. G., Mohanchandra, K. P., and Carman, G. P., "Thin film NiTi microthermostat array", ***Sensors and Actuators A: Physical,*** 13(2): 37-41 (2006).

88. Lu, J., Newaz, G. M. and Gibson, R. F., "The role of adhesive in the mechanical response of adhesively bonded aluminum hat sections under axial compression", ***International Journal of Solids and Structures,*** 41(17): 4757-4767 (2004).

89. Internet: "Mechanical Properties of Materials: Stress and Strain", **https://www.linearmotiontips.com/mechanical-properties-of-materials-stress-and-strain/ (**2019).

90. Internet: "JMNitinol technical properties", **https://matthey.com/en/products-and-services/medical-components/resource-library/nitinol-technical properties/** (2020).

91. Internet: "Chemistry learner", **https://www.chemistrylearner.com/nitinol. html**/ (2020).

92. Internet: "Corrosion and Biocompatibility", **http://www.memry.com/ resources /faq-corrosion.php**/ (2020).

RESUME

Abubaker J. Amir IRHAYIM was born in Tamzawa in 1973 and he graduated primary, elementary, and high school in this city, after that, he started an undergraduate program at Higher Institute for Comprehensive Profession Shore, Brak Al-Shshati , Department of Mechanical Engineering in 2009. Then in 2019, he started at Karabuk University Mechanical Engineering to complete his M. Sc. education.